

FOUNDED
1950
BY
M. G. M. M.

DOE/SF/11999-1
(DE86000273)

Chemical Additives for Improving Steamflood Performance

Annual Report
January - December 1984

By
L. L. Handy

March 1986

Performed Under Contract No. AT03-84SF11999

University of Southern California
Los Angeles, California



National Petroleum Technology Office
U.S. DEPARTMENT OF ENERGY
Tulsa, Oklahoma

DISCLAIMER

This report was prepared as an account of work sponsored by an agency of the United States Government. Neither the United States Government nor any agency thereof, nor any of their employees, makes any warranty, expressed or implied, or assumes any legal liability or responsibility for the accuracy, completeness, or usefulness of any information, apparatus, product, or process disclosed, or represents that its use would not infringe privately owned rights. Reference herein to any specific commercial product, process, or service by trade name, trademark, manufacturer, or otherwise does not necessarily constitute or imply its endorsement, recommendation, or favoring by the United States Government or any agency thereof. The views and opinions of authors expressed herein do not necessarily state or reflect those of the United States Government.

This report has been reproduced directly from the best available copy.

Chemical Additives for Improving Steamflood Performance

**Annual Report
January - December 1984**

**By
L. L. Handy**

March 1986

Work Performed Under Contract No. AT03-84SF11999

**Prepared for
U.S. Department of Energy
Assistant Secretary for Fossil Energy**

**Gary Peterson, Project Manager
San Francisco Operations Office
Fossil Energy Division
1333 Broadway
Oakland, CA 94612**

**Prepared by
University of Southern California
Petroleum Engineering Department
Los Angeles, CA 90089**

ABSTRACT

The extent of caustic reaction with silica at elevated temperatures was investigated under static and batch conditions in fired Berea cores. Significant progress has been made but the ultimate pH which can be perpetuated through the reservoir in a solution buffered with dissolved silica has not as yet been established as a function of the many fluid and reservoir properties which determine that pH.

Displacement experiments have shown that pH in excess of 11 will recover waterflood residual oil for specific Long Beach crudes. Recoveries at pH less than 11 may be obtained with buffered solutions containing carbonates in addition to silicates.

The measurement of relative oil and water permeabilities at elevated temperatures and reduced interfacial tensions has been completed and the results are summarized. Increasing temperature at normal interfacial tensions gives relative permeabilities which appear characteristic of more water wet systems. Decreased interfacial tensions, on the other hand, give results which shift the crossover points in a direction indicating less water wettability. The combination of temperature and interfacial tension reduction results in various shifts in the observed relative permeabilities measured. The results of these relative permeability measurements have been correlated for use in reservoir simulators.

The development of the chemical steam stimulators continues. Although this is proving to be, as anticipated, a complicated problem, progress is being made.

TABLE OF CONTENTS

	page
Abstract	ii-iii
List of Tables	v
List of Figures	vi-vii
Participants	viii
Acknowledgments	ix
Introduction	1
I. Caustic Consumption	2
A. Experimental Studies	2
B. Ion Exchange Isotherms	3
C. Kinetics of Silica Dissolution	6
II. Oil Recovery From Alkaline Hot Water Floods	10
A. Caustic Floods	11
B. Sodium Metasilicate Floods	11
C. Sodium Carbonate Floods	12
D. Discussions	13
III. Relative Water and Oil Permeabilities at Elevated Temperatures and Low Interfacial Tension	15
A. Irreducible Water Saturation	16
B. Residual Oil Saturation	17
C. Relative Permeability Curves	18
D. Relative Permeability Ratios	19
E. Hysteresis Effect in Relative Permeability Curves	19
F. Summary of High Temperature and Low Interfacial Tension Results	19
IV. Simulation of Steam-Surfactant Flooding of a Petroleum Reservoir	21
References	25
Tables	27-33
Figures	34-57
List of Publications	58

LIST OF TABLES

<u>Table</u>	<u>Page</u>
1 Equilibrium Concentration of [H ⁺] and Total Dissolved Silica as a Function of pH.....	27
2 Equilibrium Concentration of [H ⁺] and Total Dissolved Silica as a Function of pH and Number of Reactions.....	28
3 Experimental Data and Results (Caustic Floods).....	29
4 Summary of High-Tension Steady-State Experiments.....	30
5 Summary of Low-Tension Steady-State Experiments.....	31
6 Unsteady-State End-Point Data.....	32
7 Coefficients for End-Point Relative Permeabilities.....	33
8 Coefficients for Relative Permeabilities.....	33

List of Figures

<u>Figure</u>	<u>Page</u>
1 Distribution of Different Silicate Species as a Function of Hydroxyl Ion Concentration at 200°C.....	34
2 Ion Exchange Isotherm for Caustic and Berea Sandstone at Different Temperatures.....	35
3 Effect of Salt Concentration on Ion Exchange of Caustic and Berea Sandstone.....	36
4 Effluent pH as a Function of Pore Volumes of 0.1 N Hydroxide Injected in Fired Berea at 150° and 180°C with a Rate of 1 ft/day.....	37
5 Effluent pH as a Function of Pore Volumes of 0.1 N Hydroxide Injected in Fired Berea Sample with Three Different Rates of Injection 5, 1 and 0.5 ft/day at 180°C.....	38
6 Log of Fraction of Hydroxide Concentration vs. Residence Time for Three Different Initial Caustic Concentrations, 0.01, 0.316, and 0.1 N at 180°C for Fired Berea Samples....	39
7 Log of Fraction of Hydroxide Concentration vs. Residence Time for 0.1 N Initial Caustic Concentration at Four Temperatures 80°, 100°, 150°, and 180°C for Fired Berea Samples.....	40
8 Hydrogen Ion Concentration vs. Time for Different Values of Available Surface Area.....	41
9 Equilibrium pH vs. Original pH for Different Temperatures..	42
10 Total Dissolved Silica vs. Original pH for Different Temperatures.....	43
11 Recovery performance and Producing pH for Runs at Different Injection pH at 52°C.....	44
12 Effect of Temperature Change on Recovery Performance and Caustic Consumption for a Run Initially at 125°C and Finally at 180°C.....	45
13 Comparison Between WOR Curves for Caustic Floods at 52°C and 180°C.....	46
14 Comparison Between Recovery Performance and Effluent pH for Sodium Metasilicate Floods at Different Injection pH and Different Tertiary Flood Rates at 180°C.....	47
15 Comparison Between WOR Curves for Sodium Metasilicate Floods at Two Different Tertiary Flood Rates at 180°C.....	48

16	Comparison Between Recovery Performances and Effluent pH for Sodium Carbonate Floods at Different Injection pH's and Different Tertiary Flood Rates at 180°C.....	49
17	Comparison Between WOR Curves for Sodium Carbonate Floods at Different Tertiary Flood Rates at 180°C.....	50
18	Comparison Between WOR Curves for Sodium Carbonate Floods at Different Injection pH's at 180°C.....	51
19	Irreducible Water Saturation vs. Temperature.....	52
20	Steady-State Residual Oil Saturation vs. Temperature.....	53
21	Steady-State Imbibition Water-Oil Relative Permeability Curves at Elevated Temperatures (Low-Tension).....	54
22	Water/Oil Relative Permeability Ratios at Elevated Temperatures (Low-Tension).....	55
23	Hysteresis Effect on Relative Permeability Curves (T=100°C, =0.117 mN/m).....	56
24	Hysteresis Effect on Relative Permeability Curves (T=175°C, =0.015 mN/m).....	57

PARTICIPANTS

Principal Investigator: L.L. Handy
Co-Investigators: E.L. Dougherty
I. Ershaghi
Y.C. Yortsos

Graduate Assistants

K. Dehghani
S. Kumar
S.A. Marinello
A. Mehdizadeh
S. Miller
S. Saneie
J. Torabzadeh

ACKNOWLEDGMENTS

The participants under the Department of Energy contract are particularly grateful to the DOE for the support which made this research possible. They acknowledge with special appreciation the advice and counsel of our project officer, Mr. Gary Peterson.

INTRODUCTION

Although the interest in surfactants has not been abandoned, much of the effort this year has been devoted to the investigation of various caustics as steamflood additives. These have included sodium hydroxide, sodium carbonates and sodium silicates. To date the silicates have been generated in situ from the interaction between caustic and silica. The high pH sodium hydroxide solutions react with reservoir rock silica. The nature of this reaction has been investigated both experimentally and theoretically. The results of these studies are included in the first portions of this report.

High pH solutions have been used in hot water floods with Wilmington crudes. These data have shown that residual crude oil can be moved at pH's in excess of 11. Total alkalinity appears also to be an important concept. The more buffered solutions have proven more effective in recovering oil.

The final portions of the report are devoted to the measurement of relative oil and water permeabilities at steam temperatures and reduced temperatures. The particular contribution this year was the measurement at both high temperature and reduced interfacial tension. These data have not appeared in the literature previously.

Finally the available data were correlated for use in the chemical-steamflood simulator. Progress on the simulator has improved significantly, but results are not as yet available.

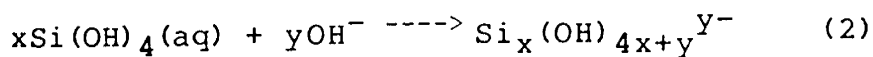
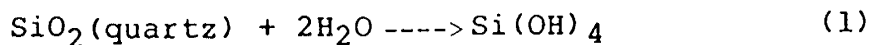
I. CAUSTIC CONSUMPTION

Caustic consumption was evaluated both experimentally and theoretically. The experiments were of two types - - dynamic experiments in Berea sandstone cores and batch experiments with disaggregated Berea sandstone. The theoretical investigations were restricted to the kinetics of solution for batch processes at temperatures somewhat in excess of room temperature.

A. Experimental Studies

An experimental study of caustic consumption in fired Berea cores was completed for temperatures from 80°C to 180°C and for caustic concentrations from 0.01 to 0.1 N. The results of these experiments have been reported¹.

Quartz goes into solution as a silicate. The reactions which result in the different silicate species are



Depending on temperature and solution pH these reactions result in a certain concentration of monomeric and multimeric silicates. The only data available are from potentiometric studies of silicate solutions at elevated temperatures by Busey and Mesmer². They found the equilibrium constant of the reactions of $\text{Si}(\text{OH})_4$

with OH^- ion for generation of $\text{SiO}(\text{OH})_3^-$ and $\text{SiO}_2(\text{OH})_2^{2-}$ and polyanion $\text{Si}_4\text{O}_6(\text{OH})_6^{2-}$ at temperatures as high as 290°C for 1 M NaCl media. Using their data on equilibrium quotients and Van Lier's equation for solubility of quartz in water one obtains³

$$\log C = 0.151 - 1162 T^{-1} \quad (3)$$

T = absolute temperature, $^\circ\text{K}$

C = $\text{Si}(\text{OH})_4$ concentration, moles/liter

with this equation along with the ionization constant of water at different temperatures, we can generate the distribution curves of silicate species at different temperatures. Note that in presence of solid silica one can assume a constant concentration of silicic acid. The curves for 200°C are shown on Figure 1.

Two factors control pH as a function of distance in the reservoir. The first of these is ion exchange. Na^+ exchanges with H^+ in solution. The second is the reaction of the OH^- with SiO_2 in the sequence of reactions discussed above. The ion exchange reactions result in a chromatographic lag in the advance of the pH front. The silicate reaction results in an overall decrease in pH which should tend towards an equilibrium value.

B. Ion Exchange Isotherms

High flow rate experiments with different caustic injection concentrations were conducted at temperatures of 80° , 100° , 150° and 180°C . An effluent hydroxide concentration versus time curve

was generated for each experiment. The amount of ion exchange was calculated by integrating this curve. Figure 2 shows ion exchange isotherms for tested temperatures. The shape of the curve suggests a Langmuir type isotherm. An increase in temperature causes an increase in the amount of ion exchange.

The effect of salt concentration on ion exchange was investigated at higher temperature (180°C) by injecting caustic solutions into the core made with three different brine solutions at concentrations of 5,000, 10,000, and 20,000 ppm. The core sample was saturated with brine of the same concentration as that used to prepare the caustic solution. The results are shown on Figure 3. One can see a qualitative decrease in the amount of ion exchange with an increase in salt concentration although the data are scattered.

During caustic flow two trends are always seen in flow experiments. First, hydroxide ion exchange breakthrough is delayed due to ion exchange and, second, the produced hydroxide ion concentration stabilizes at a level lower than the injection concentration. The difference between the effluent final hydroxide concentration and the injection concentration is caused by the silica dissolution reaction.

Flow experiments have been conducted for three injection concentrations. For every injection concentration the effect of temperature and flow rate as well as the presence of clay

minerals in the porous medium have been examined. Figures 4 and 5 show the result of this set of experiments for injection concentration of 0.1 N (pH=13). Figure 4 shows that an increase in temperature from 150° to 180°C shifted the final pH value from 12.65 to 12.00. This shows that an increase in temperature causes more dissolution. The effect of flow rate has been evaluated by conducting experiments at rates of 5.0, 1.0, and 0.5 ft/day for 180°C. Figure 5 shows the results of these experiments for injection concentration of 0.1 N. A decrease in the rate from 5 to 1 ft/day shifted the plateau from a value of 12.69 down to 12.25. At a rate of 0.5 ft/day the final pH plateau is 12.00. The results indicate that when the rate is decreased, the increased contact time between the caustic and rock results in more rock solution and corresponding lower pH's.

The rate of dissolution can be evaluated by plotting the log of hydroxide concentration versus time. A semi-log plot of the final hydroxide concentration plateau as a fraction of initial hydroxide concentration versus residence time has been generated for 180°C and three different caustic initial concentrations of 0.1, 0.0316 and 0.01 N. This plot is shown on Figure 6. This figure shows that for the lower injection concentration the data points can be approximated by a straight line. The plot also shows that there is a larger slope or higher rate of dissolution for the higher injection concentrations.

A series of flow experiments were conducted with the injection concentration of 0.1 N at four different temperatures

to investigate the effect of temperature on rate of dissolution. The results are presented on Figure 7. These experiments showed that the higher the temperature the higher the rate of dissolution as would be expected.

C. Kinetics of Silica Dissolution

A mathematical model describing the kinetics of silica dissolution was developed and tested for a batch process. We considered the dissolution mechanism to occur in two elementary steps, one involving the rapid formation of a complex (adsorbed silicic acid on the silica surface), and a slower rate-determining step that governs the partition of the complex between the silica surface and the solution. In the absence of subsequent reactions of silicic acid in solution, the mathematical model is formulated as follows:

$$\frac{dn_A}{dt} = (K_1 C_A + K_4) (n_0 - n_A) - (K_2 + K_3) n_A \quad (4)$$

$$\frac{dC_A}{dt} = [K_2 n_A - K_1 C_A (n_0 - n_A)] \frac{A}{V} \quad (5)$$

Where:

A = total silica surface (L²)

C = total dissolved silica (moles/L³)

C_A = silicic acid concentration (moles/L³)

K_i = kinetic constant (time⁻¹)

n_0 = number of available sites (m/L^2)

V = volume of solution (L^3)

When hydrolysis and ionization reactions are considered, the above equations are supplemented by a set of thermodynamic equilibrium conditions involving the various ionic species. For Equation (4) being the fast step we have

$$\frac{dn_A}{dt} = 0$$

which further implies

$$\frac{dC_A}{dt} = \frac{n_0 A K_2 K_4}{V(K_2 + K_3 + K_4)} \frac{1 - \frac{K_3 K_1}{K_2 K_4} C_a}{1 + \frac{K_1}{K_2 + K_3 + K_4}} \quad (6)$$

Equation (6) was solved analytically to determine the equilibrium value $C_{Ae} = K_2 K_4 / K_3 K_1$ and the kinetic constants K_1, K_2, K_3, K_4 . Comparison with experimental data that report equilibrium values for C_A and n_A resulted in the following kinetic constants at room temperature:⁴

$$\begin{array}{ll} K_1 = 3.49 & (\text{day}^{-1}) \\ K_2 = 1.3355 & (\text{day}^{-1}) \\ K_3 = 0.2623 & (\text{day}^{-1}) \\ K_4 = 0.6975 & (\text{day}^{-1}) \end{array}$$

We next considered the effect of the pH of the solution on the rate of dissolution and consumption. We examined the subsequent hydrolysis and ionic reactions of the silicic acid in solution following the equilibrium reaction scheme proposed by Southwick⁵. A general mathematical model was developed for the silica dissolution in a batch reactor. Seven hydrolysis and

ionization reactions were considered. The model was solved numerically using the reported values for the equilibrium constants of the hydrolysis and ionic reaction at room temperature. The following conclusions were reached:

1. Total dissolved silica increases with time, original pH level and number of active sites. It generally decreases with an increase in the number of the ionization reactions in solution. Typically, one ionization reaction predominates at lower pH, while two ionization reactions are sufficient at higher pH levels.
2. The time required for equilibrium increases significantly as the original pH level increases.
3. The equilibrium concentration is equal to K_2K_4/K_3K_1 . However, the time required for equilibrium is very sensitive to the variation in the ratio n_0A/V (Fig. 8).
4. Significant reduction of the original pH level occurs as the system approaches equilibrium.

Typical numerical results for several runs are shown in Table 1 for a dissolution process at room temperature.

The above model can be used to determine the effect of temperature on the kinetic constant, by comparison with experimental results at higher temperatures. If one uses previously reported correlations for the variation of the equilibrium constants of the two dominant ionization reactions

with temperature,^{6,7} the following values for the kinetic constants at T = 150°C available equilibrium data at higher temperatures¹ are matched approximately (in parentheses are the values obtained at 24°C).

$$K' = \frac{K_1}{K_2 + K_3 + K_4} = 0.2(1.5)$$

$$K'' = \frac{K_2 K_4}{K_2 + K_3 + K_4} = 8(0.404) \quad (\text{day}^{-1})$$

Typical values for the equilibrium hydrogen ion concentration, the total dissolved silica and the time required for equilibrium are shown in Table 2 and in Figures 9 and 10 as a function of the original pH level and the number of ionization reactions considered. It should be mentioned that the equilibrium time was determined as the value beyond which relative changes in the silicic acid concentration become smaller than 10^{-3} . It is noticed that at elevated temperatures, total dissolved silica and caustic consumption increase, particularly at low pH levels. A significant reduction in the time required for equilibrium was also observed.

A complete study of the effect of temperature on the kinetic constants is still in progress. It should be pointed out that, since present pH electrode technology does not allow for accurate pH measurements at high temperature, the available experimental data to date have been collected by measuring the pH of the solution after it has been cooled to room temperature. For a meaningful quantitative study of the effect of temperature on silica dissolution it is, then, necessary to adjust the available

experimental results to the respective values corresponding to higher temperatures. This process can be readily implemented if the temperature dependence of the equilibrium constants is known¹ and provided that the total amount of dissolved silica remains constant. The validity of the latter hypothesis is questionable, as during the cooling period some dissolved silica is expected to precipitate from the solution.

II. Oil Recovery from Alkaline Hot Water Floods

Effectiveness of alkalies such as Na_2SiO_3 and Na_2CO_3 in recovering oil were compared with results obtained earlier with NaOH . Results from core floods were evaluated with respect to recovery efficiency, water-oil ratios and alkali consumption. The results of the flood experiments are summarized on Table 3. On this table the symbols are:

$$E_{RC} = \text{recovery efficiency after high temperature alkaline flood} = \frac{S_{oi} - S_{orc}}{S_{oi}} (100) \%$$

$$E_{RR} = \text{recovery efficiency of residual oil} = \frac{S_{orw} - S_{orc}}{S_{orw}} (100) \%$$

$$E_{RW} = \text{recovery efficiency after high temperature waterflood} \\ = \frac{S_{oi} - S_{orw}}{S_{oi}} (100) \%$$

S_{oi} = initial oil saturation

$S_{o_{rc}}$ = observed residual oil saturation after high temperature alkaline flood.

$S_{o_{rw}}$ = observed residual oil saturation after high temperature waterflood

A summary of the data in this table follows.

A. Caustic Floods

Runs #1 and #2 were performed at 52°C. Injection pH's for these two runs were 13 and 12.8, respectively. Run #3 was performed at 125°C with an injection pH = 13. Tertiary flood rates were 5 ft/day for runs #1 and #2 and 7 ft/day for run #3. Run #1 recovered 37 percent of the residual oil. Recoveries for runs #2 and #3 were similar (32 percent). An increase in pH occurred after 0.76 pore volumes of caustic injection. A plateau of 12.74 was obtained. For run #3, when no more residual oil was being recovered, the flood temperature was increased from 125°C to 180°C in 24 minutes. Five pore volumes of caustic were then injected at 180°. No additional oil was recovered and the effluent pH decreased from 12.74 to 12.46 at 180°C. No pressure buildup was observed across the cores. Recovery reported as fraction of oil-in-place for runs #1 through #3 and effluent pH are plotted versus total pore volumes injected on Figures 11 and 12. The water-oil ratios at the time of oil production dropped to 5.5 and 6 for runs #2 and #3, respectively. Water-oil ratio plots for run #2 and for a run at 180°C¹¹ are given on Figure 13.

B. Sodium Metasilicate Floods

Runs #4 through #6 investigated the effectiveness of using sodium metasilicate to recover residual oil after hot waterflooding. These runs were carried out at 180°C. In run #4 no oil recovery was observed at an injection pH = 12 and at a 2 ft/day tertiary flooding rate. When the pH was changed to 13, 30.4 percent of the residual oil was recovered (run #5). In run #6, flood rate was increased to 7 ft/day. For injection pH = 13, 40.7 percent of the residual oil was recovered. No pressure buildup was observed across the cores. For run #4 effluent pH reached a value of 11.2 after 10 pore volumes of silicate injection.

An increase in pH occurred after 0.75 and 0.33 pore volumes injection of the silicate solution for runs #5 and #6. The pH plateaus were 12.55 and 12.75, respectively. Recovery as fraction of oil-in-place and effluent pH for the above three runs are plotted versus total pore volume injected on Figure 14. The water-oil ratios dropped to 6.4 and 5.8 at the time of oil production. For runs #5 and #6 oil recovery took place at lower WOR's compared to the run using caustic under the same experimental conditions. The WOR curve is shown on Figure 15. No salt was added to the alkaline solutions for runs #4 through #6.

C. Sodium Carbonate Floods

Runs #7 through #9 investigated the effectiveness of sodium carbonate on residual oil recovery after hot waterflooding at 180°C. In run #7, 13.3 percent of residual oil was recovered at

pH = 11.25. The flood rate was 2 ft/day. pH was increased to 11.45 in run #8 and as a result 18.3 percent of the residual oil was recovered. In run #9 flood rate was increased to 7 ft/day and the injection pH was kept at 11.45. 31.5 percent of the residual oil was recovered. For run #7 the injection pH was 11.25. No increase in pH occurred until 1.35 pore volumes of sodium carbonate were injected. The maximum obtained in the effluent was 10. In run #8, an increase in pH occurred after 1 pore volume of injection. In run #9, an increase in pH occurred after 0.7 pore volume injection. pH plateau values were 10.1 and 10.25 for runs 8 and 9, respectively. Recovery as a fraction of oil-in-place and the effluent pH for the above three runs are plotted versus total pore volume injected on Figure 16. Water-oil ratio dropped to 19, 6 and 7.4 at the time of tertiary oil production for runs 6 through 8. Oil production took place at higher WOR's compared to floods using caustic at the same experimental conditions. WOR curves for runs #7 through #9 are shown on Figures 17 and 18. No salt was added to the alkaline solution for runs #7 through #9.

D. DISCUSSIONS

Interfacial tensions between alkaline solutions and the Long Beach acidic crude oil increased with increasing temperature. This is due to more complete extraction from the interface at higher temperatures of the surfactant formed from the reaction of the acidic components in the oil with the hydroxide ion in the alkaline solution. This extraction process is discussed in terms of the role of desorption by Ramakrishnan and Wasan ⁹ who have

proposed the following desorption kinetics for caustic crude oil system:

$$\frac{-dn_A^-}{dt} = k_2(n_A^-) \exp\left(-\frac{W}{RT}\right)$$

This effect of temperature on the desorption rate seems to be higher for caustic than sodium metasilicate and sodium carbonate solutions. For this reason, at higher temperatures the same values of IFT can be obtained for lower pH values of sodium metasilicate and sodium carbonate when compared to those obtained for caustic. The values reported in this study are non-equilibrium IFT values but the equilibrium values are even higher. We observed this in IFT measurements with the spinning drop method.

Useful alkalinity of the alkaline solutions, which is important to the success of the oil recovery process, decreases through consumption and ion exchange with the rock and reservoir fluids. These losses are higher at higher temperatures. As a result, IFT inside the core is not constant.

Presence of higher IFT's and consumption of alkalies at higher temperatures make emulsification and entrainment and/or emulsification and coalescence possible recovery mechanisms. Although shear rate and interfacial tension are important parameters, viscosity ratio of the continuous and discontinuous phases is an important factor, also. Our estimates of viscosity ratios at temperatures of 52, 125 and 180°C are 64, 8.6 and 2.8, respectively. Ease of emulsification increases as the ratio decreases. Since at higher temperatures the viscosity ratio

decreases, floods at higher temperatures may yield satisfactory recoveries due to the greater ease of emulsification.

No recovery of the residual oil took place using caustic at pH = 13 for a tertiary flood rate of 2 ft/day at 180°C. 18 percent recovery of the residual oil was observed when 20,000 ppm salt was added. On the other hand, floods at 2 ft/day recovered residual oil using sodium metasilicate and sodium carbonate. No salt was needed for these two alkalies. Although oil recovery obtained from sodium carbonate is lower than that with sodium metasilicate at 180°C, recovery took place at lower pH values than those required for sodium metasilicate.

Consumption of these alkalies is a strong function of temperature and flood rates. For high tertiary flood rate (7 ft/day) at 180°C, 56, 35 and 6 percent of the initial OH⁻ ion was present at the effluent for sodium metasilicate, caustic and sodium carbonate, respectively. These values dropped to 30, 10, and 5.6 percent when the rate was decreased to 2 ft/day. Injection pH was 13 for sodium metasilicate and caustic. For sodium carbonate it was 11.45. No matter what alkali was injected, oil was produced with the injected chemicals and no significant oil bank was formed.

III. Relative Water and Oil Permeabilities at Elevated Temperatures and Low Interfacial Tension

Steady-state imbibition and drainage relative permeabilities for high and low tension systems were obtained experimentally on

fired Berea sandstone at temperatures from 22°C to 175°C.¹⁰ All experiments were conducted at 300 psig fluid pressure and 650 psig overburden pressure. The core and fluid properties and summary of experimental results for high and low tension systems are given in Tables 4 and 5, respectively. For the low-tension system, the oil was n-dodecane with a surfactant solution of 0.2 wt.percent. Petrostep 465 in 1 wt.percent NaCl brine was used as the aqueous phase. The two phases were equilibrated prior to experiment. Steady-state experiments were conducted using an experimental procedure discussed in an earlier report. Both imbibition and drainage relative permeability curves were generated to investigate the hysteresis effect. Relative permeabilities were calculated based on the absolute permeability of the core. Experimental results on the combined effects of temperature and interfacial tension on residual saturations and relative permeability curves are discussed in the following sections.

A. Irreducible Water Saturation

Irreducible water saturations obtained at different temperatures are shown in Figure 19. These saturations were established by injecting 50 pore volumes of oil at 120 cc/hr. For the high-tension system, irreducible water saturation increased from 28 percent pore volume at 22°C to 38 percent at 175°C. Upon increasing oil flow rate to 200 cc/hr, no more water was produced at low temperatures. At high temperatures, the additional water produced was less than 1 percent pore volume.

In addition, the irreducible water saturation obtained at the end of the drainage cycle for steady-state experiments at any temperature was within 0.5 percent pore volume of the S_{wir} established by oil flood. This indicates that capillary end effect was not significant for the system and that the observed increase in irreducible water saturation with temperature was not due to changes in viscous forces only as reported by Sufi et al.¹¹ The increase in S_{wi} with temperature suggests an increase in water wetness of the sandstone with increasing temperature.

For the low-tension system, the changes in S_{wir} with temperature were not significant, but, at all temperatures, irreducible water saturation for low tensions were lower than those at high tensions. This suggests that the increase in temperature and decrease in IFT have opposite effects on S_{wir} . Increasing temperature, increases S_{wir} but lowering of IFT decreases S_{wir} . Therefore, it is speculated that the irreducible water saturation in the low-tension system at elevated temperatures is controlled by the IFT level and wettability changes due to temperature.

B. Residual Oil Saturation

Residual oil saturations obtained at the end of the steady-state imbibition cycles are plotted vs. temperature on Figure 20 for both high- and low-tension systems. S_{or} decreased with increasing temperature for both systems but the reduction was much greater for the low-tension system. Residual oil saturation decreased from 33 percent PV at 22°C to 25 percent at 175°C for the high-tension system. The reduction for the low-tension

system was from 23 percent at 27°C to 2 percent at 175°C. The large decrease in the S_{Or} for the low-tension system is mainly caused by the reduction of interfacial tension with increasing temperature (0.187 mN/m at 27°C to 0.015 mN/m at 175°C). Increasing temperature and decreasing IFT both favor reduction of residual oil. A significant reduction in S_{Or} was observed at IFT values less than 0.117 mN/m corresponding to temperatures above 100°C) showing a synergistic effect of temperature and interfacial tension in mobilizing residual oil. This is also an indication that S_{Or} in water/oil system can be greatly affected by IFT values less than 10^{-1} mN/m at elevated temperatures. Residual oil saturations obtained by unsteady-state displacement experiments given in Table 6 are slightly higher than those of the steady-state.

C. Relative Permeability Curves

The relative permeability curves for the low-tension system at different temperatures are shown in Figure 21. Relative permeability to both phases, at a given saturation, increases with increasing temperature up to 100°C. Above 100°C relative permeability to oil still increases while relative permeability to water decreases in the middle range of saturations. Relative permeability to water at residual oil saturation is still higher for higher temperatures. A possible explanation of the decrease in k_{rw} at temperatures above 100°C could be the change in wettability of the rock as indicated by the shift in the crossover point toward higher water saturations. Increase in water-wetness opposes the effect of reduced IFT on relative

permeability to water. Comparing the relative permeability curves for high- and low-tension systems at a given temperature, it can be shown that relative permeability to both oil and water increases as the interfacial tension decreases.

D. Relative Permeability Ratios

Water/oil relative permeability ratios for low-tension systems at different temperatures are shown in Figure 22. k_{rw}/k_{ro} decreases with increasing temperature at a given saturation.

E. Hysteresis Effect in Relative Permeability Curves

Hysteresis was observed in relative permeability curves for both wetting and nonwetting phases at low tensions and elevated temperatures as shown in Figures 23 and 24. The effect appeared to be more pronounced for the nonwetting phase (oil) at any temperature. The hysteresis effect was more significant at lower temperatures and higher IFT's and decreased with increasing temperature and decreasing IFT. The effect disappeared at 175°C for the low-tension system. Secondary drainage relative permeabilities were lower than imbibition relative permeabilities for both oil and water. However, first drainage relative permeabilities (starting with a 100% saturated core) were higher than imbibition values (Figure 23). Hysteresis between imbibition and secondary drainage was more pronounced at lower water saturations while the reverse was true for hysteresis between first drainage and imbibition relative permeabilities.

F. Summary of High Temperature and Low Interfacial Tension Results

Experimental results for the low-tension system indicate that with increasing temperature (decreasing interfacial tension)

- a) The relative permeability to oil increases at a given saturation.
- b) The relative permeability to water increases in a temperature range up to 100°C. Above 100°C, k_{rw} decreases in the middle range of saturations, possibly due to wettability alteration, but it is still consistently higher at S_{Or} for higher temperatures.
- c) The water/oil relative permeability ratio decreases while the curve shifts towards higher water saturations.
- d) The residual oil saturation decreases significantly due to very low IFTs.
- e) The irreducible water saturation does not change significantly, probably due to opposite effects of temperature on interfacial tension and wettability of the system.

The reduction of interfacial tension with temperature (0.19 mN/m at 22°C to 0.015 mN/m at 175°C) and the change in wettability of the rock (indicated by the shift of the crossover point of the relative permeability curves) are mainly responsible for the above results.

Comparison of the results of low-tension system with those of a high-tension system (reported earlier) shows that at a certain temperature, with decreasing IFT, the relative permeability to both oil and water increases, while both the irreducible water saturation and the residual oil saturation decrease. This is mainly caused by the reduction of capillary

forces at lower interfacial tensions.

Hysteresis between imbibition and drainage relative permeability curves was observed for both high- and low-tension systems at all temperatures. The effect decreases at higher temperatures and lower IFTs. Hysteresis was absent at 175°C (IFT of 0.015 mN/m).

IV. Simulation of Steam-Surfactant Flooding of a Petroleum Reservoir

Empirical correlations of relative permeability data at elevated temperatures and at both high and low interfacial tensions are required for the steam-chemical simulation model. These correlations have been developed to fit the data of Torabzadeh and Handy¹⁰.

Relative permeability functions can be generated using the residual saturations. The general relationship has been found by almost all investigators to be exponential in a 'normalized' saturation which, however, has been defined in several different ways. The important idea in modeling relative permeabilities is to replicate the end-point permeabilities as accurately as possible, and to approximate the region in between with standard mathematical functions.

End point relative oil permeability was correlated against the residual water saturation and the mobile water saturation range, $S_{wm} = 1 - S_{or} - S_{wr}$. The latter two parameters closely represent the nature of the system:

1. For ideal system (low IFT, high temperature), S_{wr} approaches

a very small nonzero value ϵ , and S_{wm} approaches $1 - \epsilon$. The relative oil permeability approaches 1.

2. For the high tension system, with increasing temperature, S_{wr} increases and S_{or} decreases. However, for the system we studied, S_{wm} decreases due to a smaller decrease in S_{or} with temperature. The relative oil permeability increases with increasing temperature.

3. With increasing temperature, S_{wr} increases then decreases in the low tension region, and for the system we studied, S_{wm} increases due to a significantly strong decrease in S_{or} with IFT. The relative oil permeability increases with decreasing IFT.

Thus, the end point relative oil permeabilities are directly related to residual saturation values and the mobile water saturation. The end point relative water permeabilities could also be similarly correlated, but they are more complex to relate. Increasing temperature and decreasing IFT have opposing effects on this parameter. A better relationship would be to correlate the end point relative oil to water permeability ratio, which reflects the wettability of the system and is, therefore, predictable with more certainty. From a theoretical standpoint, this ratio should decrease with increasing water wetness, i.e., with increasing temperature. Thus, the end point relative permeability ratio can also be correlated as a function of S_{wr} and S_{wm} . The equations used for fitting the end point relative permeabilities are as below:

$$k_{ro}(S_{wr}) = U^V S_{wr}^W S_{wm}$$

$$k_{ro}(S_{wr})/k_{rw}(S_{or}) = X^Y S_{wr}^Z S_{wm}$$

Table 7 shows the results of the regression analysis carried out using the data of Torabzadeh and Handy.¹⁰ The fit is quite satisfactory for most practical applications.

To generate the intermediate relative permeability values and the curvature of the permeability versus saturation relationship, we found it entirely satisfactory to use the following model first proposed by Chierici:¹²

$$k_{rw}^* = \exp(-MS_w^{**N})$$

$$k_{ro}^* = \exp(-PS_w^{**Q})$$

where M, N, P, Q are constants, and

$$k_{rw}^* = k_{rw}/k_{rw}(S_{or})$$

$$k_{ro}^* = k_{ro}/k_{ro}(S_{wr})$$

$$S_w^{**} = (S_w - S_{wr})/(1 - S_{or} - S_w)$$

Note that S_w^{**} , unlike the 'normalized' saturations used elsewhere, has a value from 0 to ∞ . This kind of relationship implicitly satisfies the end points:

(i) At $S_w = S_{wr}$, $S_w^{**} = 0$, and $k_{rw}^* = e^{-\infty} = 0$, implying that $k_{rw} = 0$, which is the condition desired.

(ii) At $S_w = 1.0 - S_{or}$, $S_w^{**} = \infty$ and $k_{rw}^* = \exp(-M \infty^N) = e^0 = 1$, implying that $k_{rw}^* = k_{rw}(S_{or})$, which is the condition desired.

Similar conclusions can easily be verified for oil relative permeability at the end points.

The correlations obtained using this model agree very well with experimental data. Table 8 outlines the results. There are no universal M, N, P, Q constants; they vary with each case considered. A close look at the variations in these constants, M, N, P, Q shows that they exhibit some sort of maxima/minima as

a function of IFT and temperature and do not follow any simplistic correlatable behavior. The data from Torabzadeh and Handy² show that the trend in the shift of the relative permeability curves with decreasing IFT and increasing temperature is not unidirectional. To suitably decipher and simulate the behavior of the complex interaction of temperature and interfacial tension, the combined effects of these two independent variables on relative permeabilities need to be studied in greater detail for a wider variety of systems. To conclude from a single study could be quite erroneous.

For the same reasons, correlations that use the capillary number, or IFT, or residual saturations, or combinations of these, fail to duplicate the relative permeability curves with acceptable accuracy. The results obtained using one such correlation by Amaefule et al.³ resulted in curve fits with an error of almost 70-80%, with certain values in the ultralow tension and high temperature range, yielding errors in excess of 250%.

The simulation model has reached the stage where all the routines worked together for the case of no fluid injection and no fluid production. This indicates that all the routines work satisfactorily, the matrix is set-up and solved correctly and the material balance equations have been properly developed and implemented. Testing has begun for fluid injection and production. The errors encountered in this portion of the simulator are generally more complex than those encountered in the no injection-no production case.

REFERENCES

1. Dehghani, K. and Handy, L.L.: "Caustic Consumption by a Sandstone at Elevated Temperatures" SPE 12767 presented at SPE California Regional Meeting, Long Beach, April 11-13, 1984.
2. Busey, R.H. and Mesmer, R.E.: "Ionization Equilibrium of Silicic Acid and Polysilicate Formation in Aqueous Sodium Chloride Solutions to 300°C," *Inorganic Chemistry*, Vol. 16, no. 10 (1977) 2444-2450.
3. Van Lier, J.A.: "The Solubility of Quartz," Drukkerijen Uitgeversmij V/h Kemink en Zoom n.v. Dom Plein, Utrecht, Netrecht, Netherlands, 1965.
4. Stoher, W.: "Formation of Silicic Acid in Aqueous Suspensions of Different Silica Modifications," *Adv. in Chem. Series*, 67 (1967) 161-182.
5. Southwick, J.G.: "Solubility of Silica in Alkaline Solutions: Implications for Alkaline Flooding," SPE 12771, presented at SPE California Regional Meeting, April 11-13, 1984, Long Beach, CA.
6. Rejzendo: "Determination of Hydrolysis of Sodium Silicate and Calculation of Dissolution Constant of Orthosilicic Acid at Elevated Temperatures," *Geo. Khimiya* 2, 161-169 (in Russian) *Geochem. Int.* 4, 99-107 (English translation).
7. Vanlier, J.H., Debrayn, P.L. and Overbeck, Th. G.: "The Solubility of Quartz," *J.Phys. Chem.* 64, 1675-1682, (1960).
8. Mehdizadeh, A. and Handy, L.L.: "Displacement Studies of Viscous Oil from Consolidated Cores using Caustic at Temperatures above 125°C," SPE 12040 presented at SPE 58th Annual Technical Meeting, San Francisco, CA, October 5-8, 1983.
9. Trujillo, E.M.: "The Static and Dynamic Interfacial Tensions Between Crude Oils and Caustic Solutions," *Soc. Pet. Eng. J.* (August 1983) 645-656.
10. Torabzadeh, S.J. and Handy, L.L.: "The Effect of Temperature and Interfacial Tension on Water/Oil Relative Permeabilities of Consolidated Sands" SPE 12689 presented at the SPE/DOE Fourth Symposium on EOR in Tulsa, OK. April 15-18, 1984.
11. Sufi, A.S., Ramey, H.J., Jr. and Brigham, W.E.: "Temperature Effects on Relative Permeabilities of Oil-Water Systems," paper SPE 11071 presented at the SPE 57th Annual Technical Conference and Exhibition, New Orleans, Sept. 26-29, 1982.
12. Chierici, G.L.: "Novel Relations for Drainage and Imbibition

Relative Permeabilities" paper, SPE 10165 presented at the SPE 56th Annual Technical Conference and Exhibition, San Antonio, TX, Oct 5-7, 1981.

Table 1

Equilibrium Concentration of $[H^+]$ and Total Dissolved
Silica as a Function of pH

	Total Dissolved Silica (moles/lit)	Equilibrium Concentration of $[H^+]$ (mole/lit)	Time
9	1.32424×10^{-4}	4.129607×10^{-9}	34
10	2.004216×10^{-4}	4.130569×10^{-10}	40
11	8.813080×10^{-4}	4.118146×10^{-11}	92
11.5	2.523015×10^{-3}	1.308572×10^{-11}	320
12.0	7.687502×10^{-3}	4.104911×10^{-12}	626
12.5	2.388777×10^{-2}	1.273×10^{-12}	1568
13.0	7.151269×10^{-2}	3.998928×10^{-13}	4720

$T = 24^{\circ}C$

$K' = 1.53$

$K'' = 0.404 \text{ (day}^{-1}\text{)}$

$\frac{An^0}{V} = 90.0 \text{ } \mu\text{g/m}$

Table 2
Equilibrium Concentration of [H⁺] and Total
Dissolved Silica as a Function of pH
and Number of Reactions

Original pH	Number of Reactions Considered	Total Dissolved Silica (mole/l)	Equilibrium [H] (mole/l)	Time (day)
13.5	1	0.2864051	3.090884×10^{-11}	98
13	1	9.230293×10^{-2}	9.776351×10^{-11}	38
12.5	1	3.091952×10^{-2}	3.091675×10^{-10}	18
12	1	1.150841×10^{-2}	9.776740×10^{-10}	10
11.5	1	5.370078×10^{-3}	3.091681×10^{-9}	8
11	1	3.428974×10^{-3}	9.776676×10^{-9}	8
13.5	2	0.1778490×10^{-2}	2.260018×10^{-10}	28
13	2	2.315930×10^{-2}	$4.2547702 \times 10^{-10}$	24
12.5	2	2.299180×10^{-2}	8.363627×10^{-10}	14
12	2	9.731996×10^{-3}	1.766838×10^{-9}	10
11.5	2	5.048601×10^{-3}	4.153302×10^{-9}	8
11	2	3.383475×10^{-3}	1.103967×10^{-8}	8

T = 150°C

K' = 0.2

K" = 8 (day⁻¹)

$\frac{An^0}{V} = 90.9 \text{ } \mu\text{g/m}$

TABLE 3 - EXPERIMENTAL DATA AND RESULTS

Run #	k (md)	PV (cc)	Inj. Solution (Secondary)	Inj. Solution (Tertiary)	Flood Sec. (ft/D)	Flood Tert. (ft/D)	Flood Temp. (°C)	S _{oi}	S _{orw}	S _{orc}	E _{RW} %	E _{RC} %	E _{RR} %	Alkali Break-through (PV)	pH Plateau
SS1-1	682	118	Brine 2%	NaOH pH = 13 Salt = 0%	7	5	52	.705	.361	.22	48.8	68.8	37	.67	12.8
SS1-2	675	118	Brine 2%	NaOH pH = 12.8 Salt = 0%	7	5	52	.741	.339	.229	54	69	32	.56	12.6
SS2-3	640	118.5	Brine 2%	NaOH pH = 13 Salt = 0%	7	7	125	.671	.354	.242	47	64	32	.76	12.74
SS3-4	672	117.5	Brine 2%	Na ₂ SiO ₃ pH = 12 Salt = 0%	7	2	180	-	-	-	-	-	0	10.0	11.2
SS4-5	653	118	Brine 2%	Na ₂ SiO ₃ pH = 13 Salt = 0%	7	2	180	.6	.368	.256	39	57	30.4	.75	12.55
SS4-6	632	118	Brine 2%	Na ₂ SiO ₃ pH = 13 Salt = 0%	7	7	180	.58	.346	.205	40	64.6	40.7	.33	12.75
SS5-7	627	119	Brine 2%	Na ₂ CO ₃ pH = 11.25 Salt = 0%	7	2	180	.582	.309	.268	47	54	13.3	1.35	10.0
SS5-8	630	118	Brine 2%	Na ₂ CO ₃ pH = 11.45 Salt = 0%	7	2	180	.591	.316	.258	46.5	56.4	18.3	1.0	10.1
SS6-9	636	118	Brine 2%	Na ₂ CO ₃ pH = 11.45 Salt = 0%	7	7	180	.575	.292	.2	49.2	65.2	31.5	.7	10.25

TABLE 4 - SUMMARY OF HIGH-TENSION STEADY-STATE EXPERIMENTS

Run #	T °C	k # µm ²	cm ³ /hr	µ _o mPa-s	µ _w mPa-s	ρ _o g/cm	ρ _w g/cm	σ mN/m	S _{wl} %	S _{or} %	S _{wcd} %	End-Point Relative Perm.		
												k _{ro} at S _{wl}	k _{rw} at S _{or}	k _{ro} at S _{wcd}
16A	22	0.950	30	1.4250	0.9782	0.7531	1.0047	33.6	27.8	33.9	28.0	0.631	0.106	0.521
17A	22	0.957	60	1.4250	0.9782	0.7531	1.0047	33.6	27.7	33.2	27.9	0.706	0.087	0.576
17B	22	0.957	120	1.4250	0.9782	0.7531	1.0047	33.6	27.9	31.7	28.0	0.713	0.089	0.587
18A	51	0.926	60	0.9520	0.5520	0.7382	0.9938	33.2	32.7	30.8	32.6	0.725	0.085	0.638
19A	100	0.910	120	0.5270	0.2895	0.7115	0.9651	30.3	35.8	28.9	36.1	0.740	0.083	0.696
19B	100	0.910	180	0.5270	0.2895	0.7115	0.9651	30.3	36.1	27.5	36.3	0.740	0.091	0.704
19C	100	0.910	60	0.5270	0.2895	0.7115	0.9651	30.3	36.3	28.0	36.6	0.704	0.085	0.650
20A	150	0.920	120	0.3352	0.1875	0.6825	0.9249	24.7	36.3	26.7	36.1	0.848	0.094	0.800
20B	150	0.920	180	0.3352	0.1875	0.6825	0.9249	24.7	36.1	26.7	-	0.845	0.081	-
22A	175	0.910	120	0.2752	0.1588	0.6706	0.9004	20.4	38.5	25.6	38.5	0.930	0.074	0.879
22B	175	0.910	180	0.2752	0.1588	0.6706	0.9004	20.4	39.9	24.8	39.7	0.859	0.064	0.789
23A	150	0.816	120	0.3352	0.1875	0.6825	0.9249	24.7	36.3	26.5	36.3	0.876	0.080	0.817
23B	150	0.816	180	0.3352	0.1875	0.6825	0.9249	24.7	36.3	26.3	36.2	0.847	0.074	0.775
23C	150	0.816	60	0.3352	0.1875	0.6825	0.9249	24.7	36.2	28.0	37.4	0.740	0.054	0.692

*Experiments conducted on Core #BS-5: L = 21.60 cm, A = 5.07 cm², φ = 24.3%, PV = 26.6 cm³

TABLE 5 - SUMMARY OF LOW-TENSION STEADY-STATE EXPERIMENTS

Run #	T °C	Core #	φ %	PV cm ³	k μm ²	q _t cm ³ /hr	μ _o mPa-s	μ _w mPa-s	ρ _o g/cm ³	ρ _w g/cm ³	σ mN/m	S _{wl} %	S _{or} %	S _{wcd} %	End-Point Rel. Perm.		
															k _{ro} at S _{wl}	k _{rw} at S _{or}	k _{ro} at S _{wcd}
24A	27	BS-6	24.30	26.6	0.629	120	1.3300	0.8951	0.7473	1.0019	0.187	21.3	23.6	21.5	0.823	0.190	0.748
25A	51	BS-6A	24.30	26.6	0.514	120	0.9520	0.5658	0.7345	0.9934	0.165	22.9	18.3	22.6	0.850	0.240	-
26A	26.7	BS-7	24.57	26.9	0.948	120	1.3330	0.8999	0.7474	1.0020	0.187	21.8	20.1	-	0.801	0.219	-
27A	100	BS-7A	24.57	26.9	0.938	120	0.5270	0.2967	0.7089	0.9636	0.117	24.1	5.6	23.3	0.847	0.676	0.759
29A	150	BS-8	24.57	26.9	0.819	120	0.3352	0.1922	0.6826	0.9245	0.050	23.3	3.5	23.6	0.929	0.602	0.872
30A	175	BS-8	24.57	26.9	0.809	120	0.2752	0.1628	0.6715	0.8973	0.015	21.1	2.3	21.0	1.000	0.913	0.986
31A1	100	BS-8A	24.57	26.9	0.775	120	0.5270	0.2967	0.7089	0.9636	0.117	100.0	-	23.3	-	1.000	0.861
31A2	100	BS-8A	24.57	26.9	0.775	120	0.5270	0.2967	0.7089	0.9636	0.117	23.4	6.0	23.4	0.861	0.667	0.846

*Dimension of all cores: L = 21.60 cm, D = 2.54 cm, A = 5.07 cm²

TABLE 6 - UNSTEADY-STATE END-POINT DATA

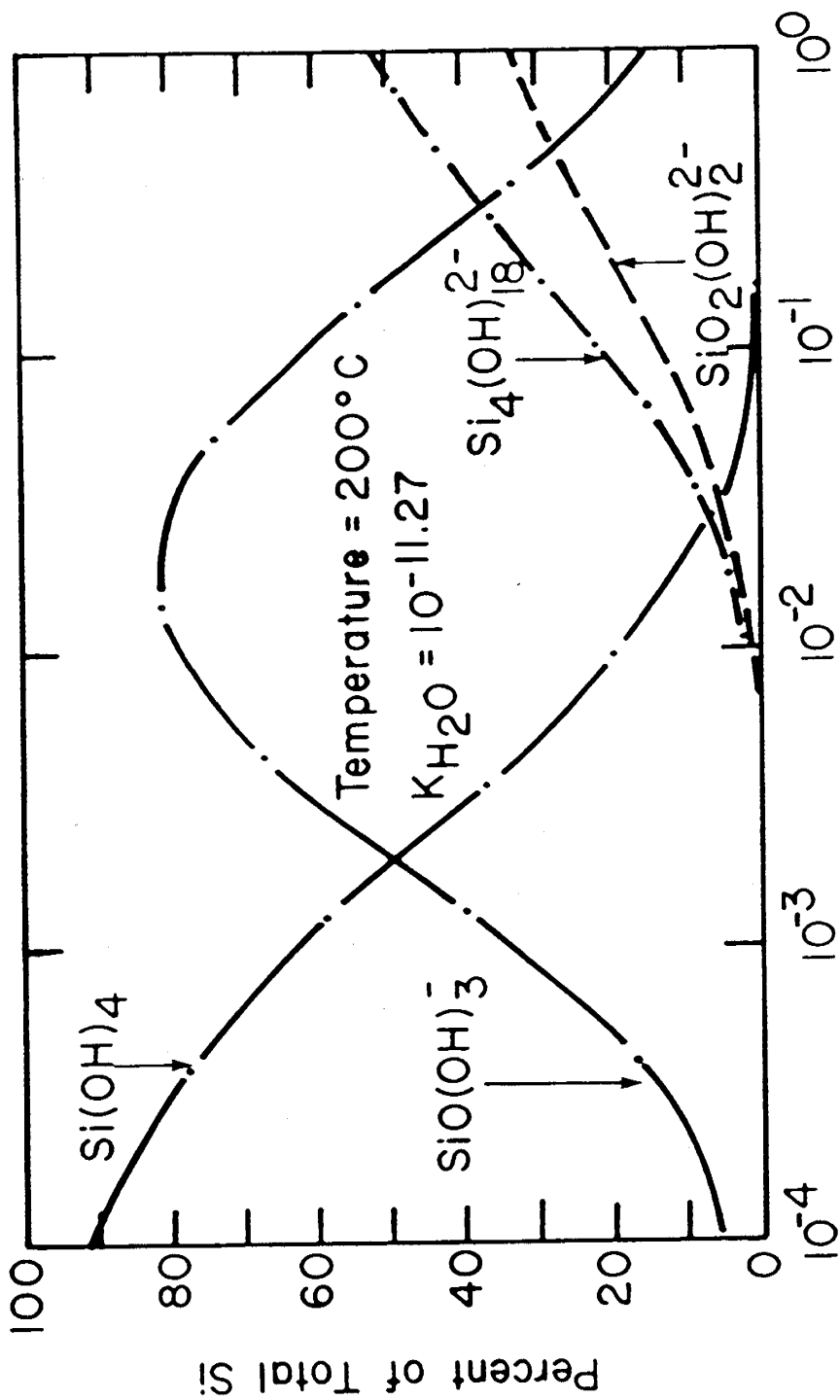
Run #	T °C	Core #	q_t cm ³ /hr	σ mN/m	S_{wl} %	S_{or} %	k_{ro} at S_{wl}	k_{rw} at S_{or}
21C	26	BS-5	120	33.4	30.4	34.4	0.662	0.095
190	100	BS-5	120	30.3	36.4	30.1	0.696	0.084
23D	150	BS-5	120	24.7	37.5	28.2	0.780	0.069
22C	175	BS-5	120	20.4	39.7	27.0	0.855	0.064
26C	26.7	BS-7	120	0.187	22.0	25.0	0.779	0.217
27C	100	BS-7A	180	0.117	23.9	8.1	0.789	0.592
29C	150	BS-8	180	0.050	23.5	5.3	0.806	0.551
30C	175	BS-8	180	0.015	21.5	3.6	0.950	0.788

TABLE 7 : Coefficients for End-point Relative Permeabilities

FOR	COEFFICIENTS	RES. SUM OF SQUARES	ST. DEV.
$k_{ro}(S_{wr})$	$U = 2.3136, V = 0.49684, W = 0.53469$	0.03269	0.0361
$k_{ro}(S_{wr})/k_{rw}(S_{or})$	$X = 0.12423, Y = -0.88298, Z = -3.4126$	0.20669	0.0982

TABLE 8 : Coefficients for Relative Permeabilities

T	IFT	M	N	P	Q	RES. SUM OF SQUARES	
						WATER	OIL
22	33.6	0.862550	0.719850	1.320100	0.465620	0.2049E-04	0.2038E-02
51	33.2	1.263844	0.679430	0.975609	0.675500	0.9590E-04	0.3555E-02
100	30.3	1.487805	0.921840	0.900854	0.711040	0.7224E-04	0.5524E-03
150	24.7	1.895688	0.886160	1.031071	0.682590	0.4178E-04	0.1475E-02
175	20.4	1.668699	0.550060	0.881612	0.599080	0.3690E-03	0.6195E-02
27	0.187	1.573349	0.468350	2.557017	0.821530	0.2449E-03	0.5211E-02
51	0.165	1.411201	0.492470	2.055394	0.914590	0.2853E-02	0.9666E-02
100	0.117	0.669958	0.867850	0.716122	0.660820	0.2322E-02	0.6844E-02
150	0.050	1.012500	0.732370	0.688937	0.670450	0.1355E-01	0.4804E-02
175	0.015	1.436809	0.643660	0.704069	0.643220	0.3232E-01	0.6827E-02



Hydroxyl Ion Concentration, Moles/Liter

Figure 1 Distribution of different silicate species as a function of hydroxyl ion concentration at 200°C

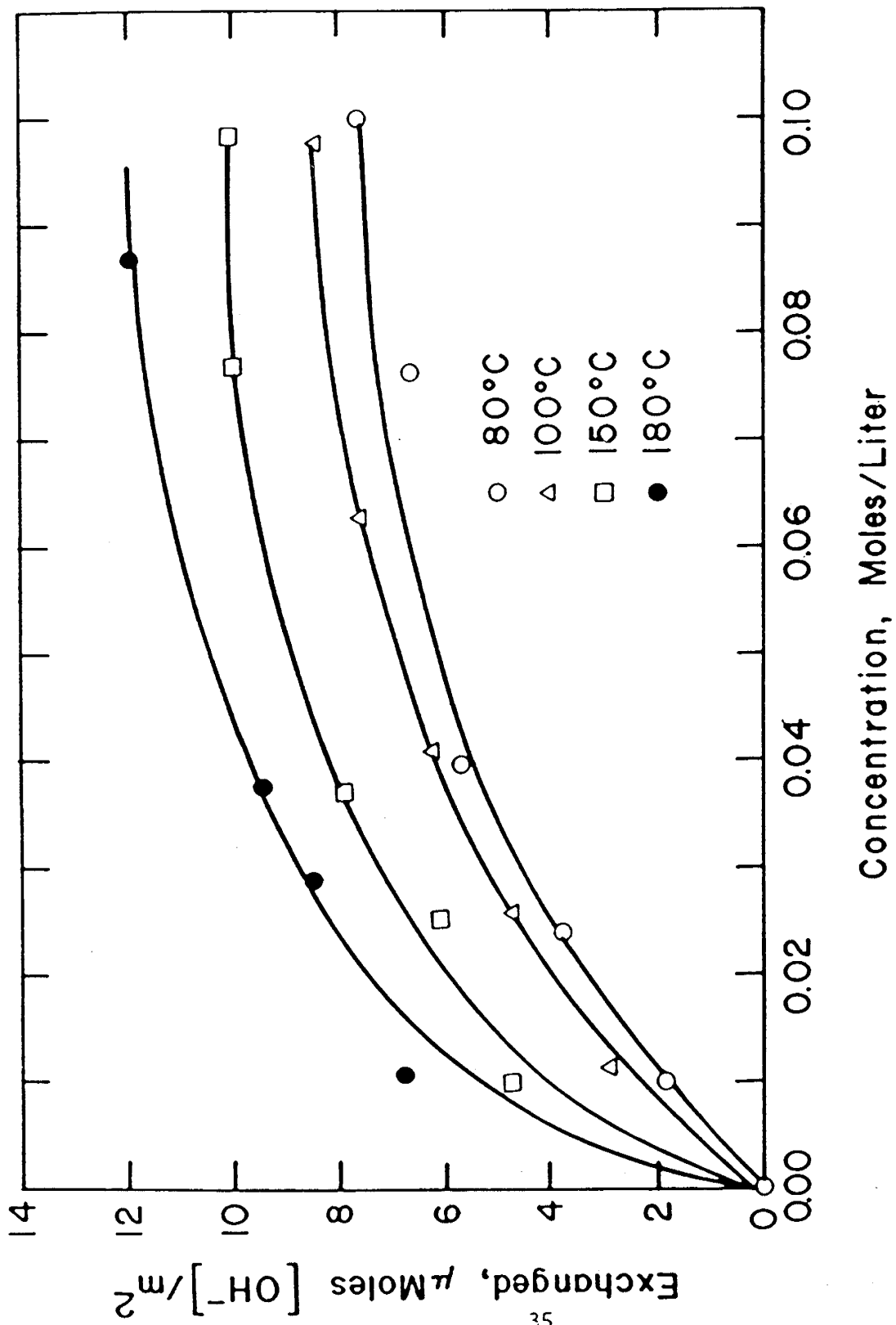


Figure 2 Ion exchange isotherm for caustic and Berea sandstone at different temperatures

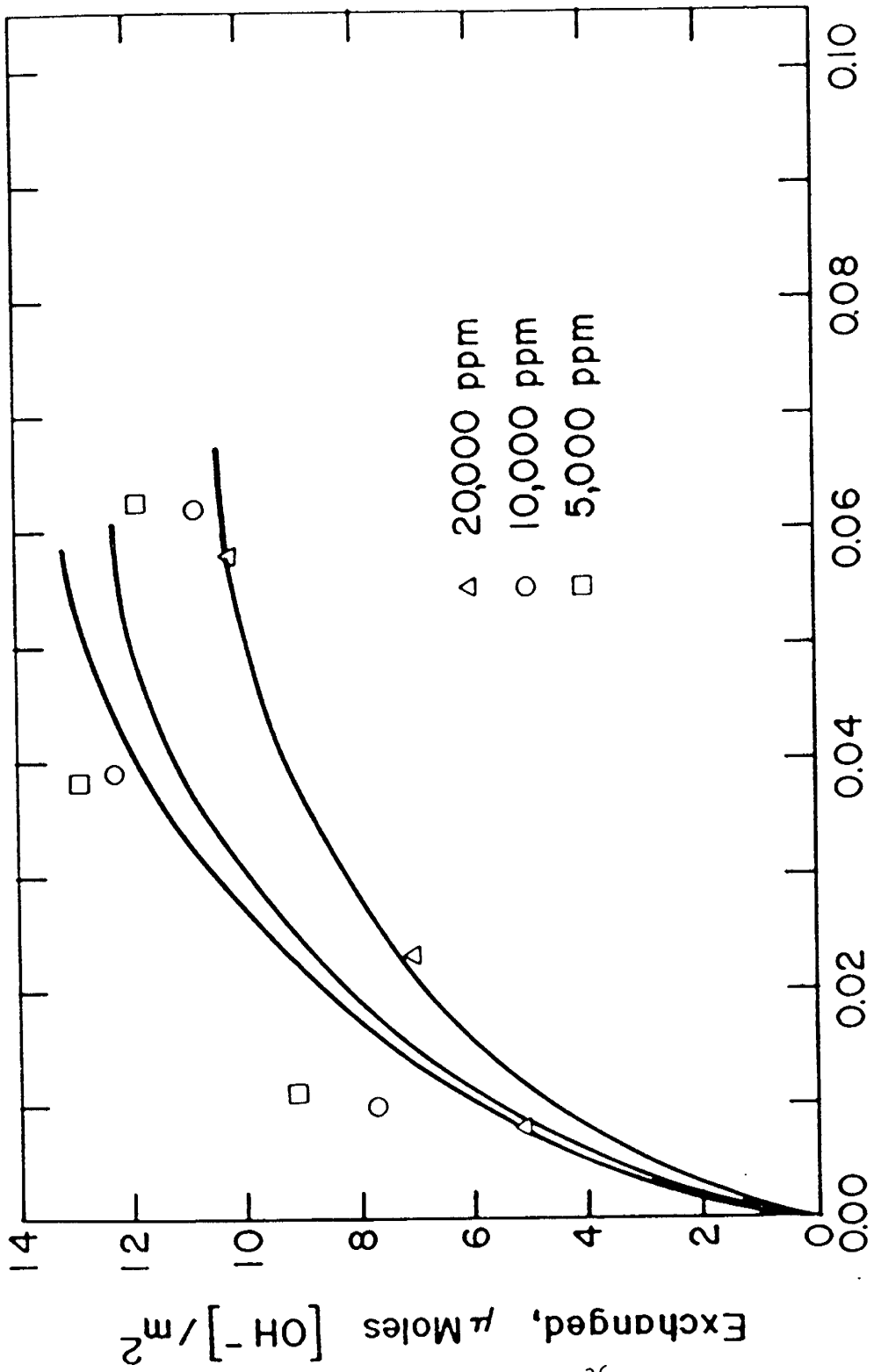


Figure 3 Effect of salt concentration on ion exchange of caustic and Berea sandstone

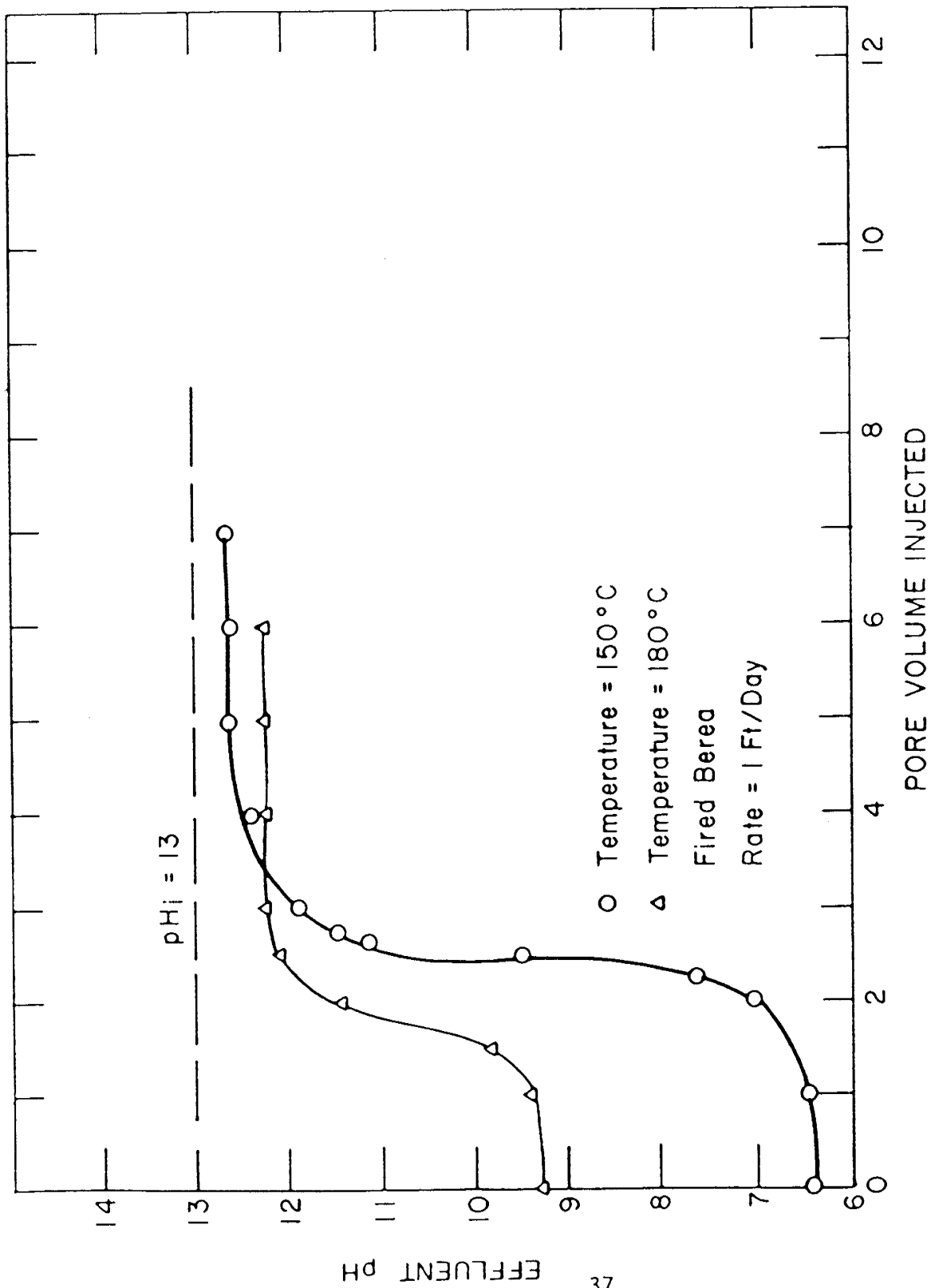


Figure 4 Effluent pH as a function of pore volumes of 0.1 N hydroxide injected in fired Berea at 150° and 180°C with a rate of 1 ft/day

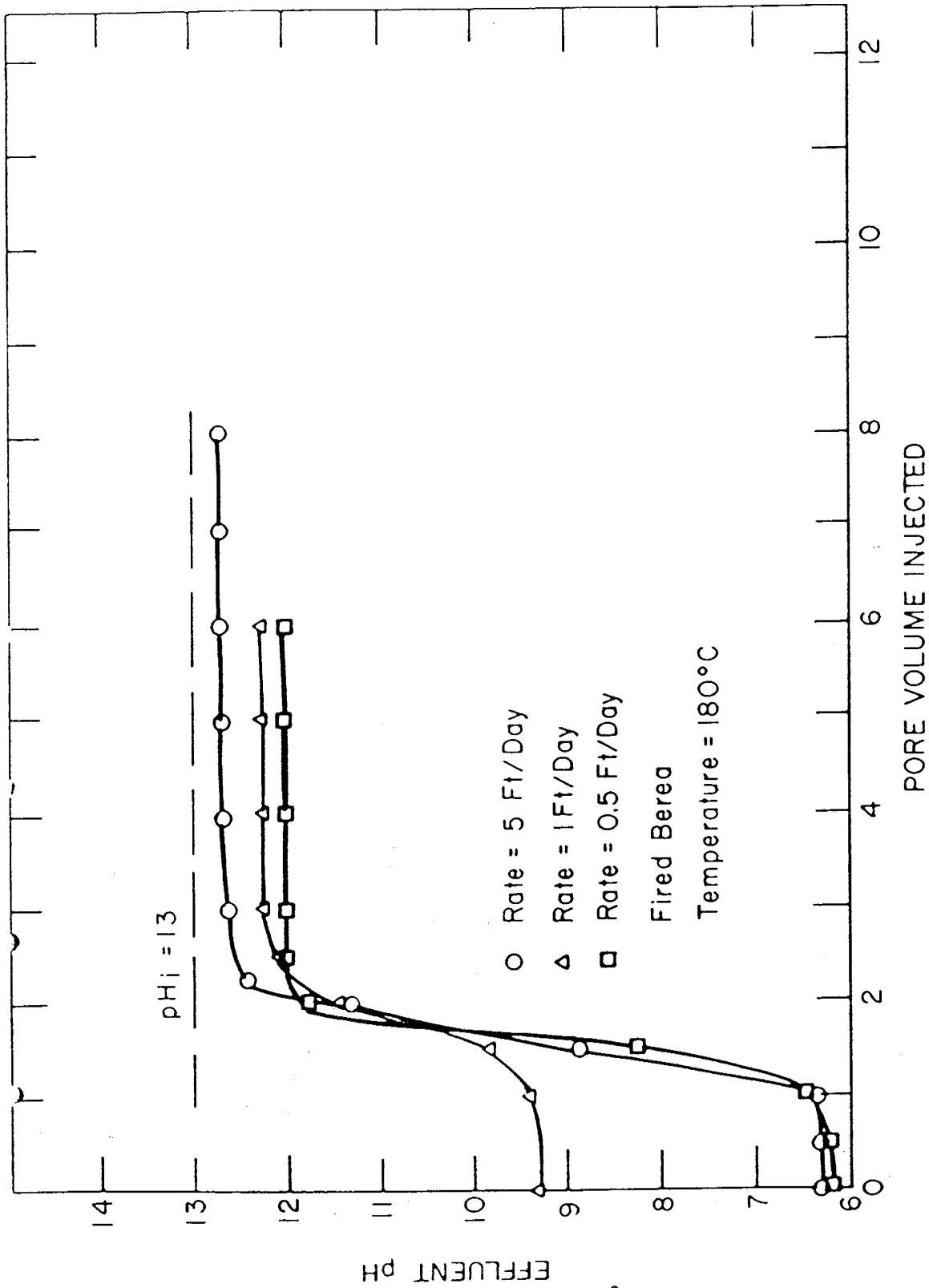


Figure 5 Effluent pH as a function of pore volumes of 0.1 N hydroxide injected in fired Berea sample with three different rates of injection 5, 1 and 0.5 ft/day at 180°C

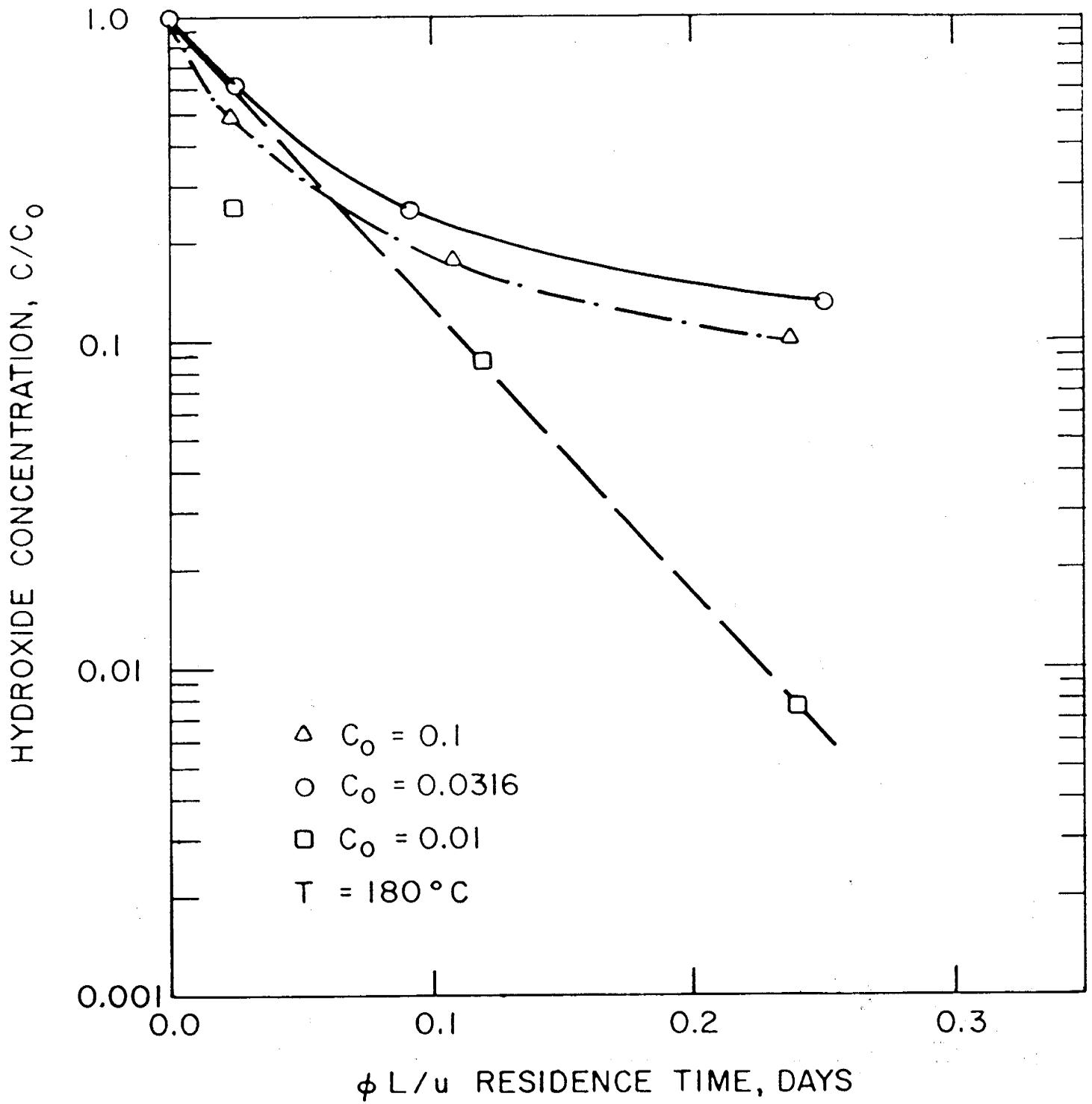


Figure 6 Log of fraction of hydroxide concentration vs. residence time for three different initial caustic concentrations, 0.01, 0.316, and 0.1 N at 180°C for fired Berea samples

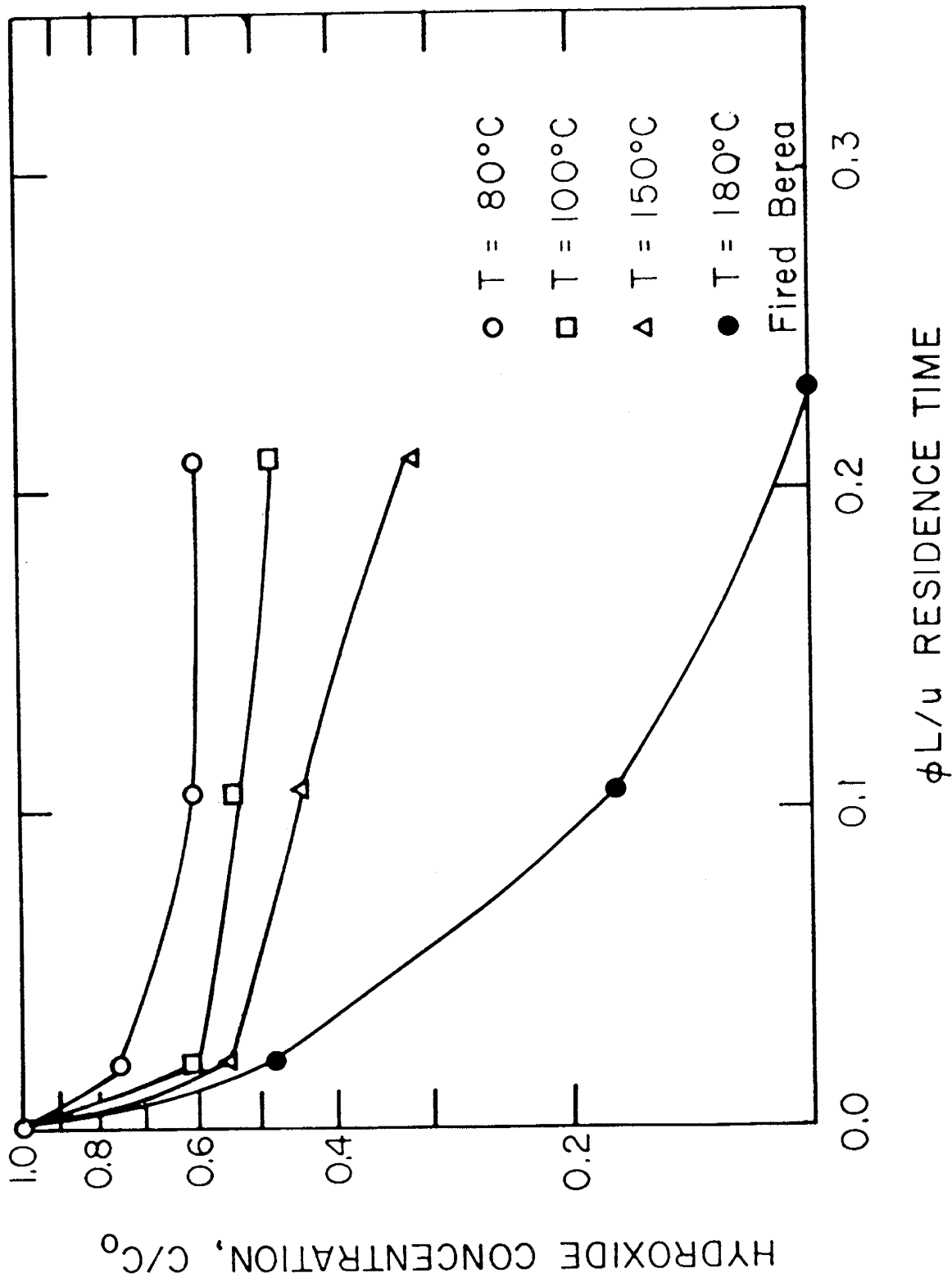


Figure 7 Log of fraction of hydroxide concentration vs. residence time for 0.1 N initial caustic concentration at four temperatures 80°, 100°, 150°, and 180°C for fired Berea samples

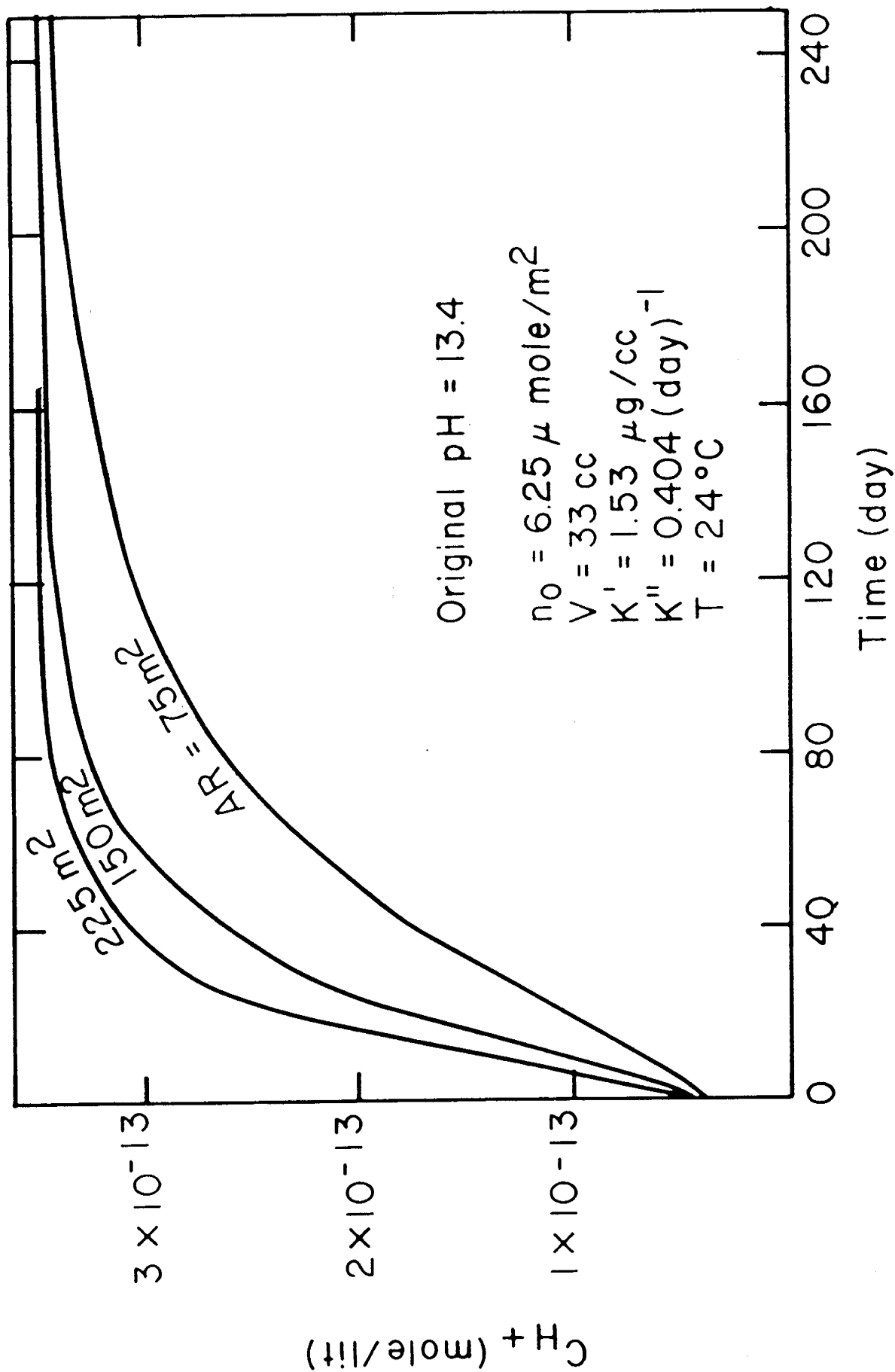


Figure 8 Hydrogen ion concentration vs. time for different values of available surface area

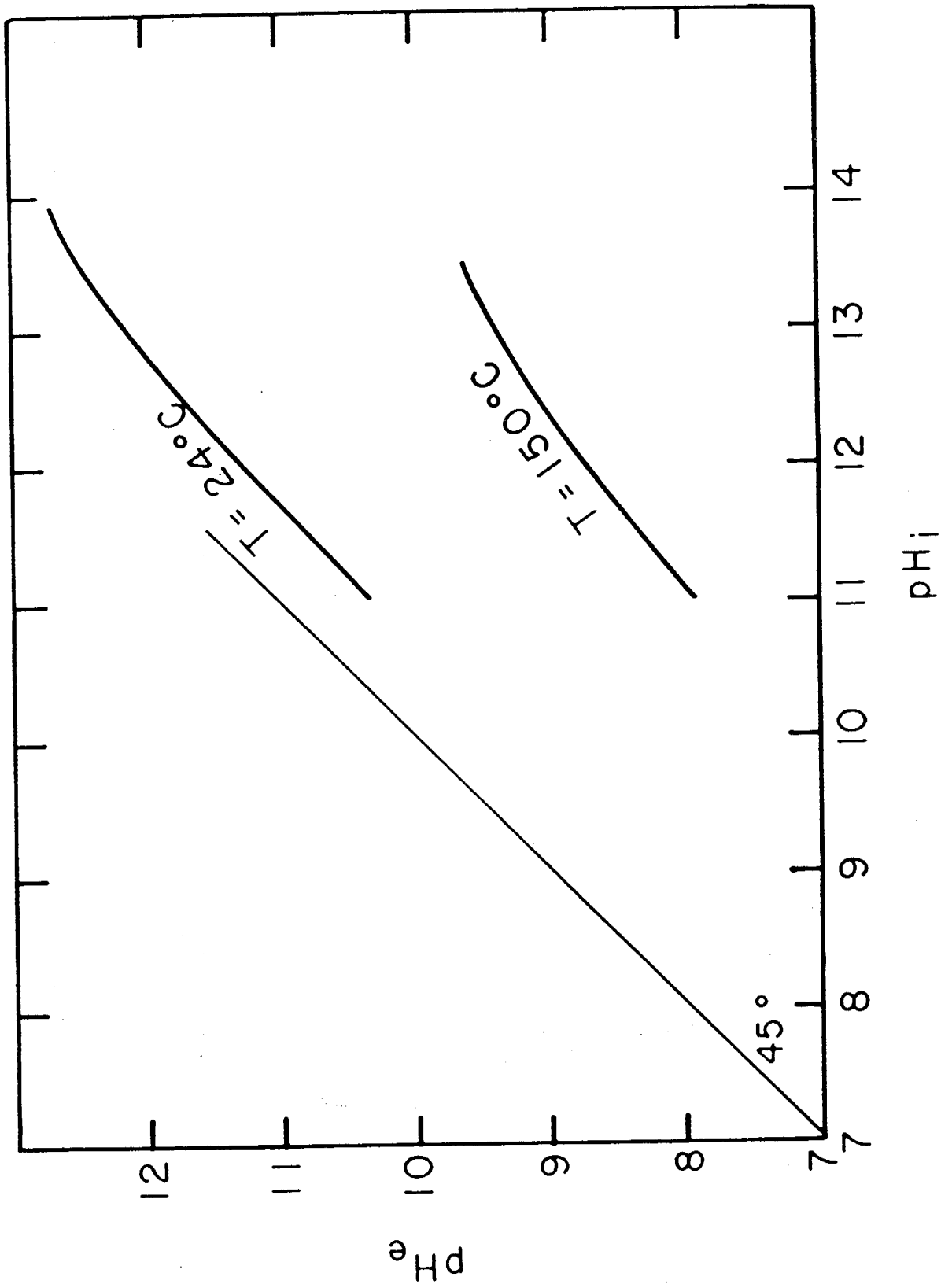


Figure 9 Equilibrium pH vs. original pH for different temperatures

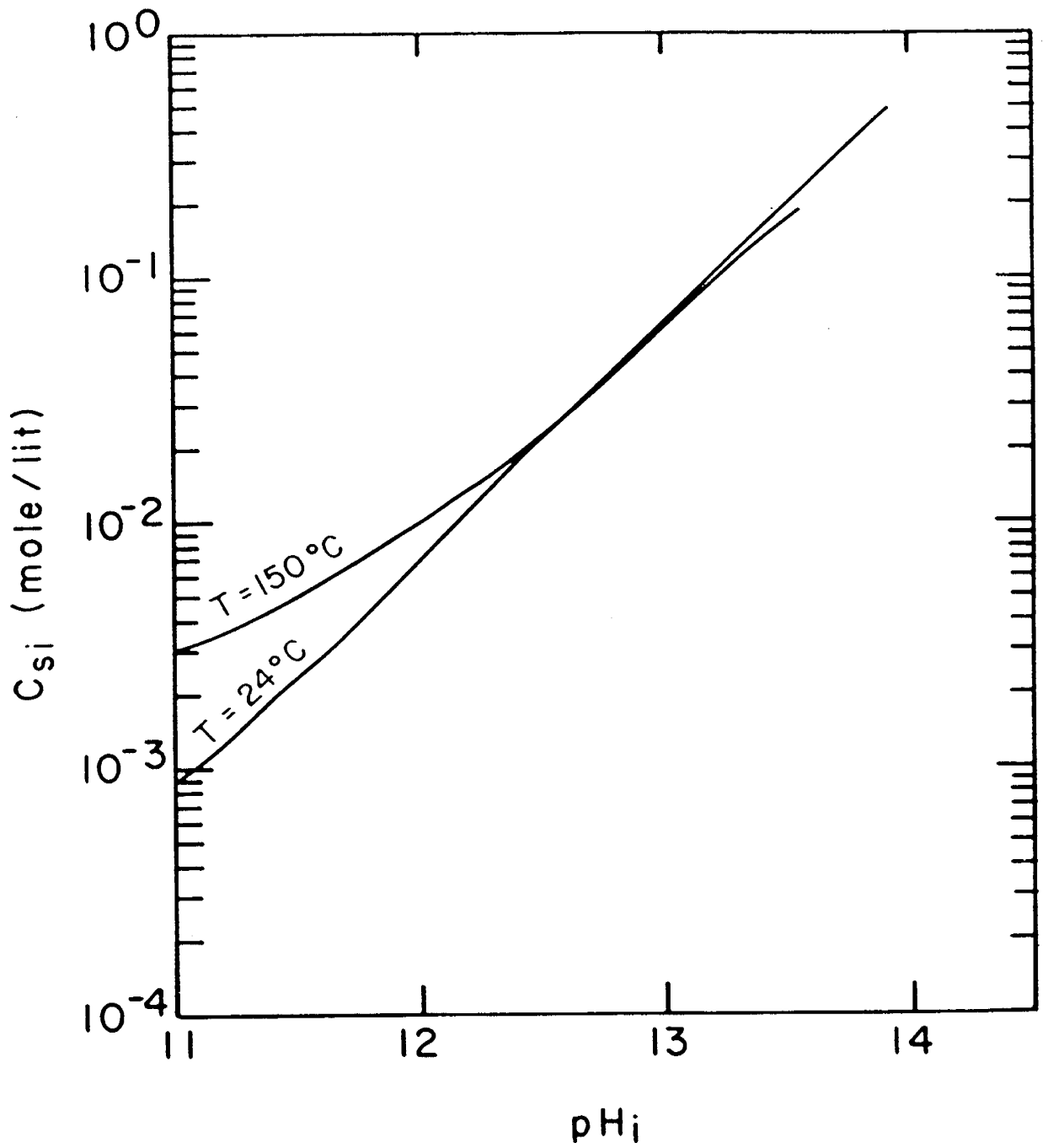


Figure 10 Total dissolved silica vs. original pH for different temperatures

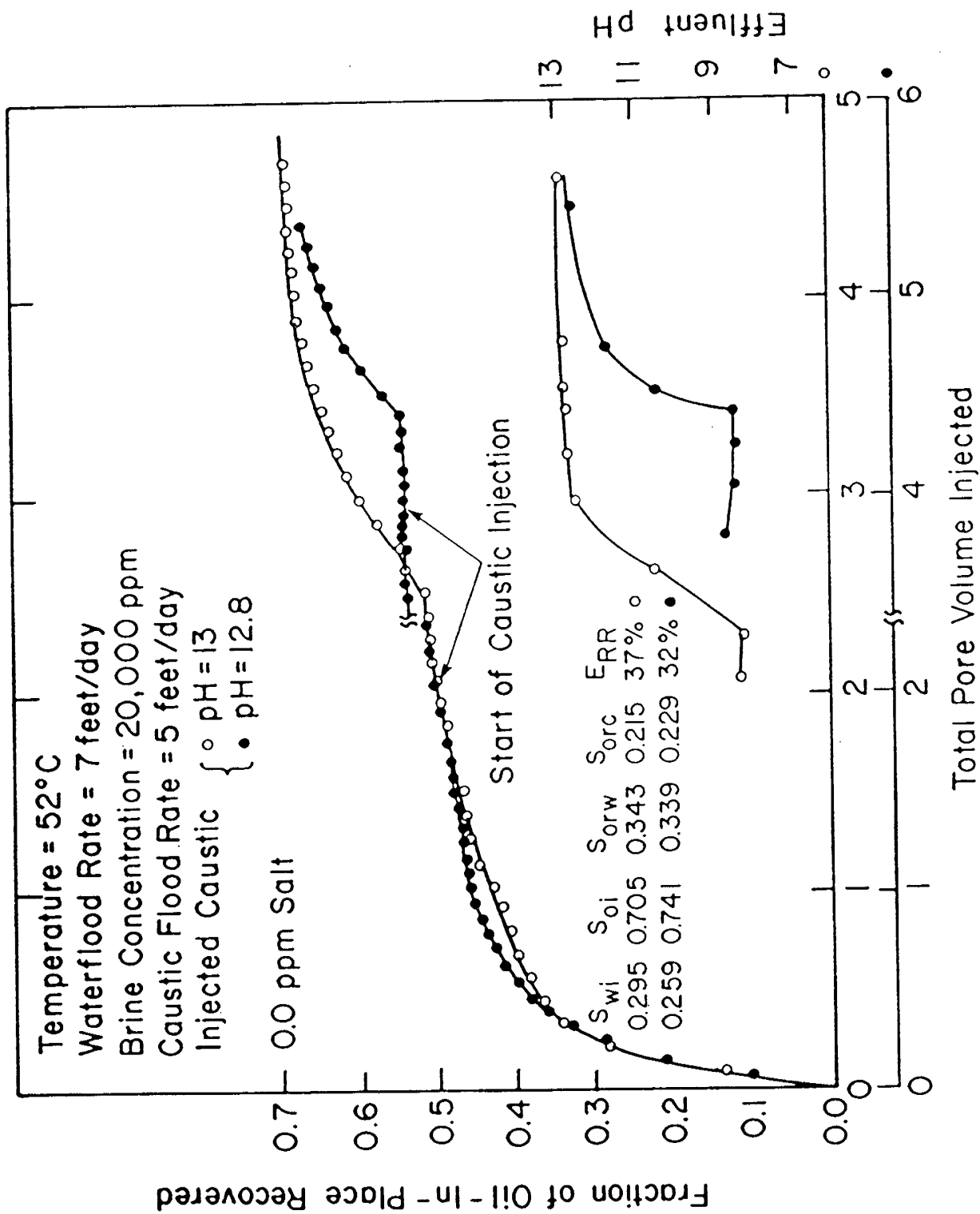


Figure 11 Recovery performance and producing pH for runs at different injection pH at 52°C

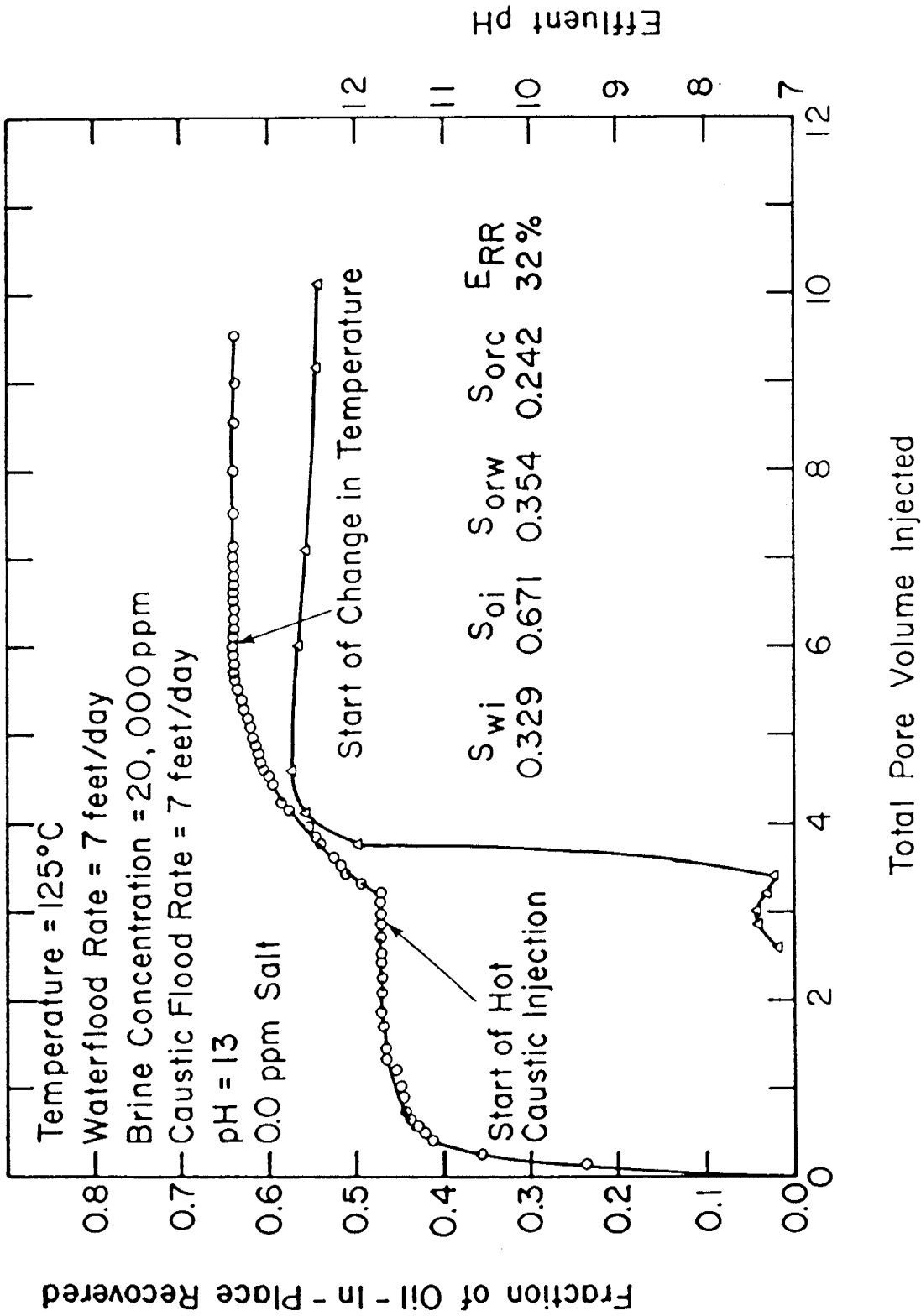


Figure 12 Effect of temperature change on recovery performance and caustic consumption for a run initially at 125°C and finally at 180°C

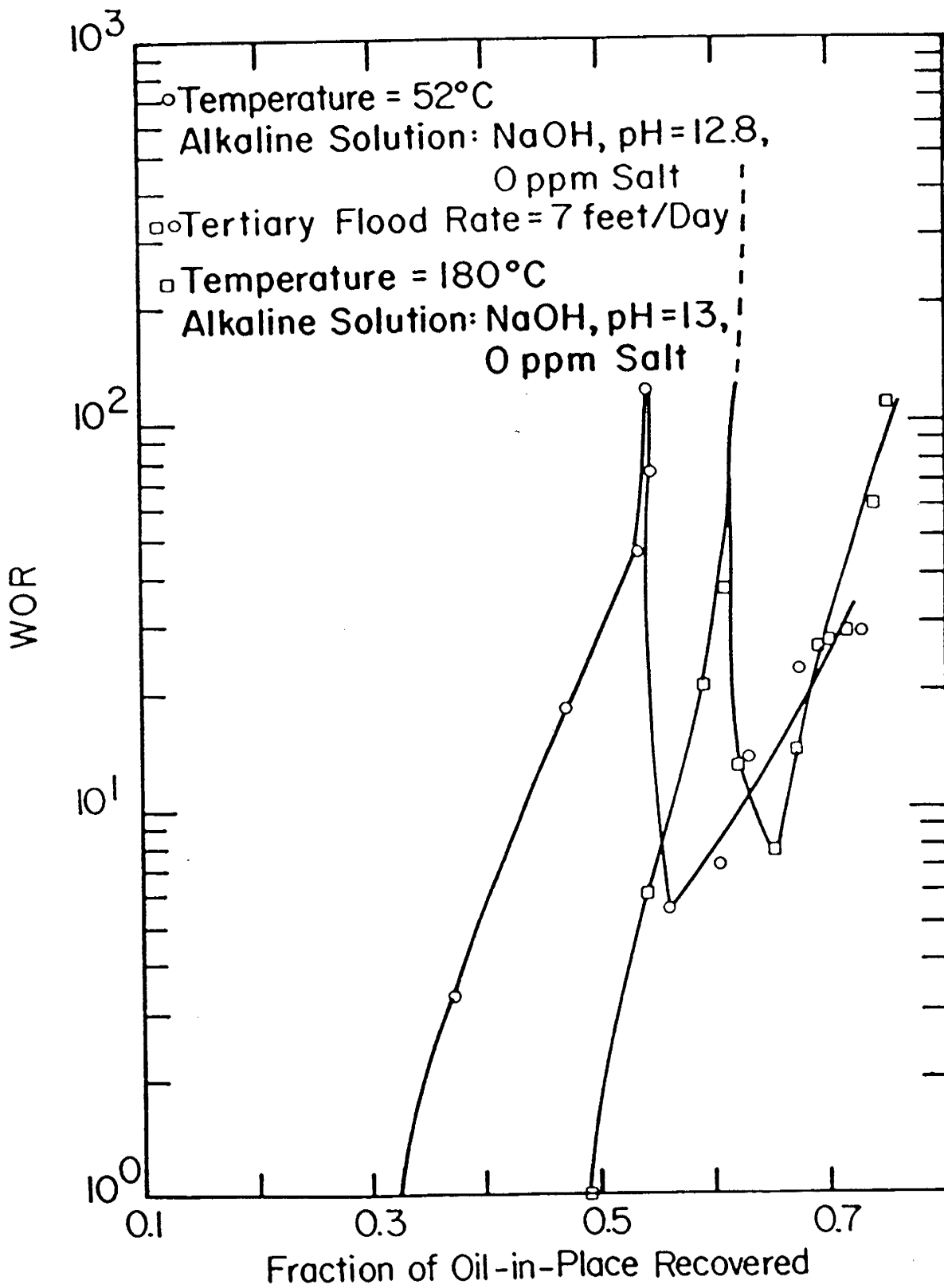


Figure 13 Comparison between WOR curves for caustic floods at 52°C and 180°C

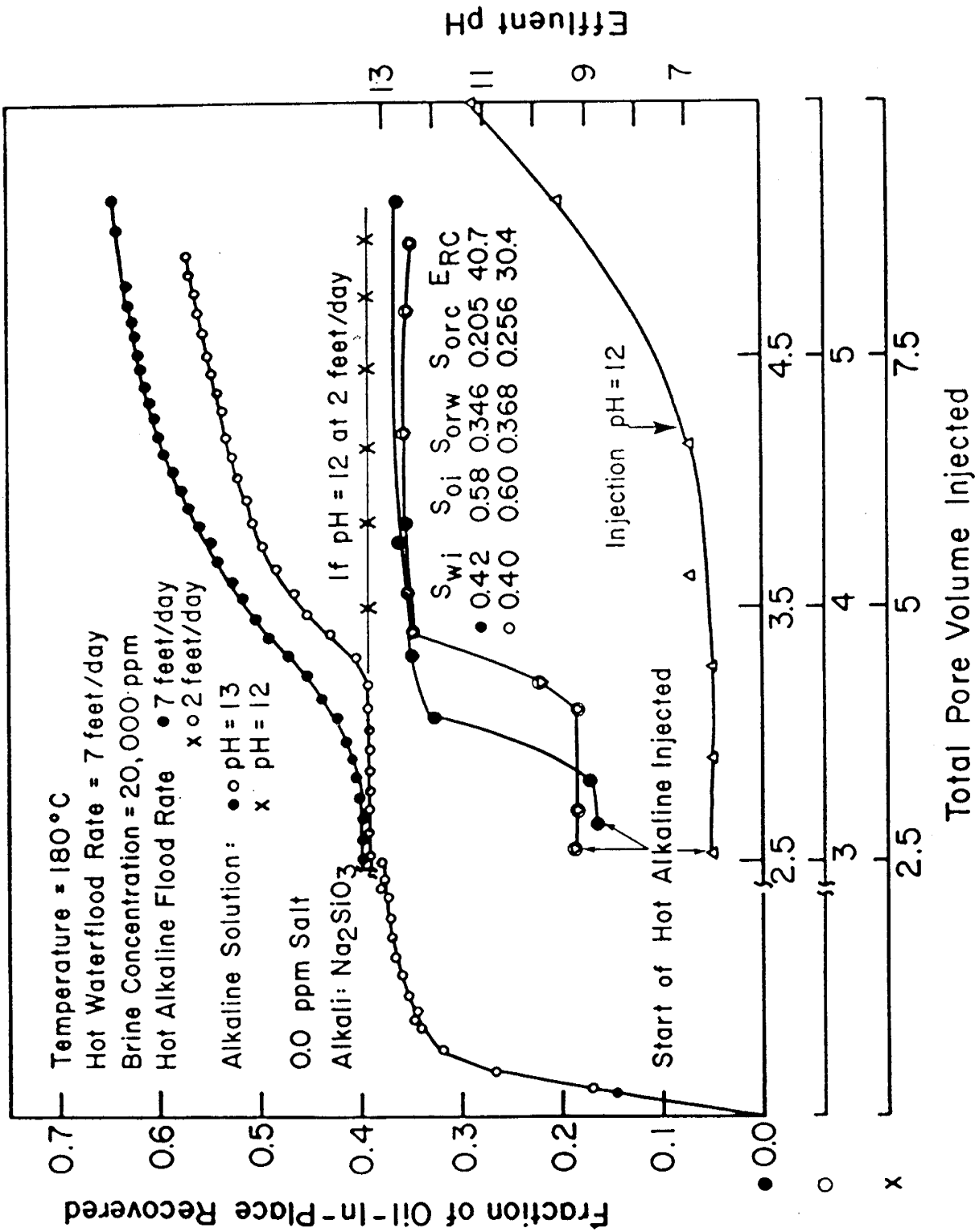


Figure 14 Comparison between recovery performance and effluent pH for sodium metasilicate floods at different injection pH and different tertiary flood rates at 180°C

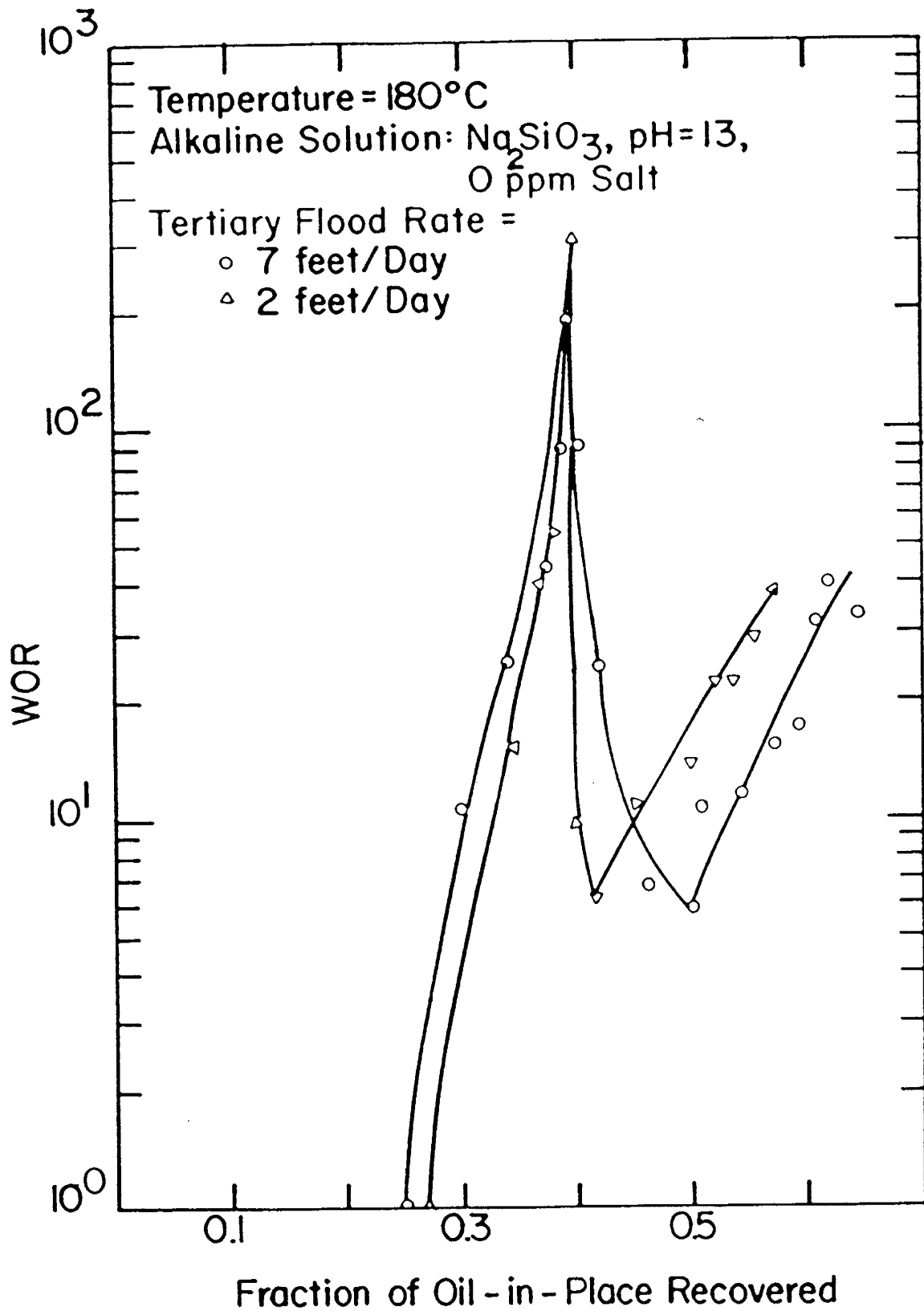


Figure 15 Comparison between WOR curves for sodium metasilicate floods at two different tertiary flood rates at 180°C

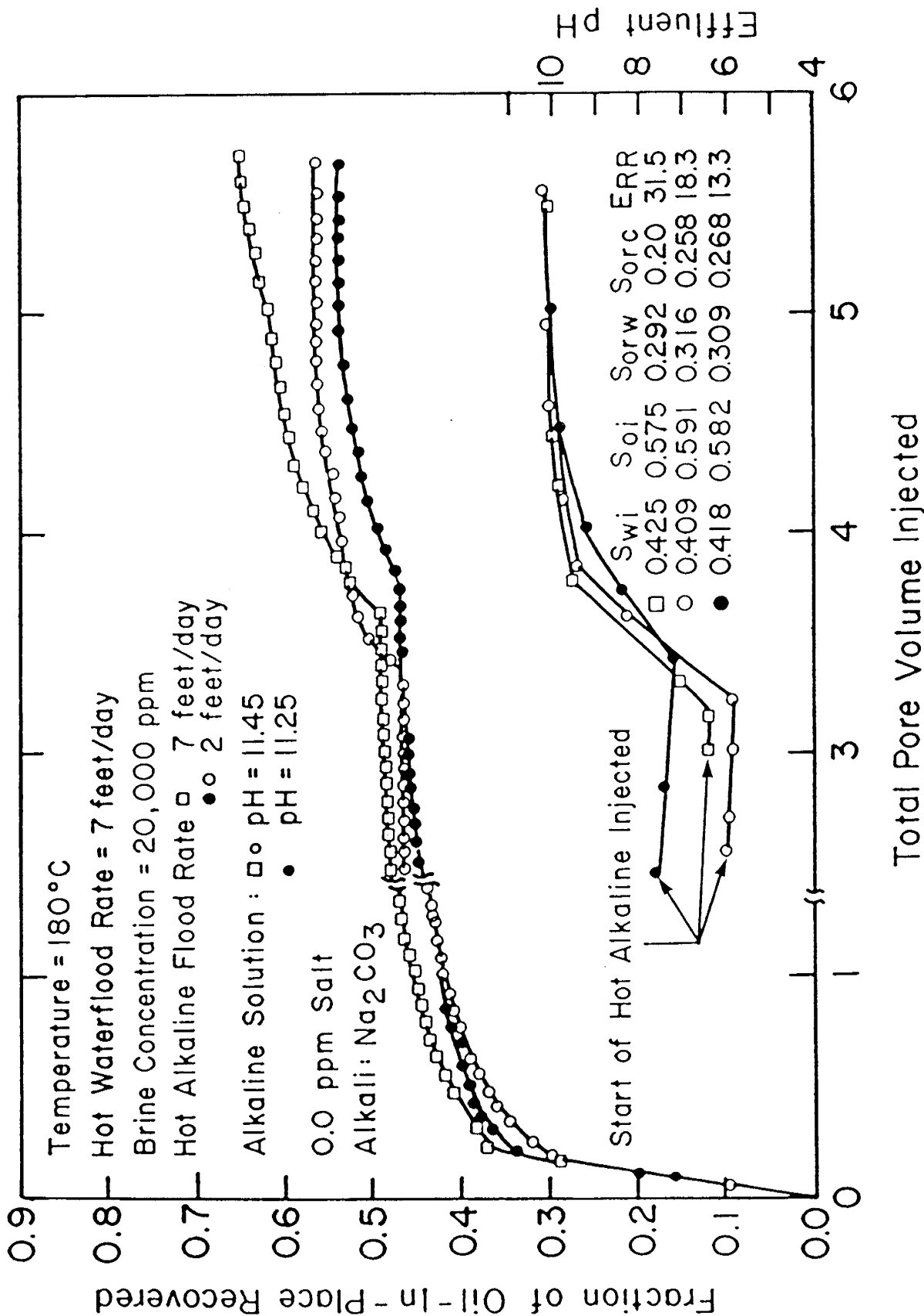


Figure 16 Comparison between recovery performances and effluent pH for sodium carbonate floods at different injection pH's and different tertiary flood rates at 180°C

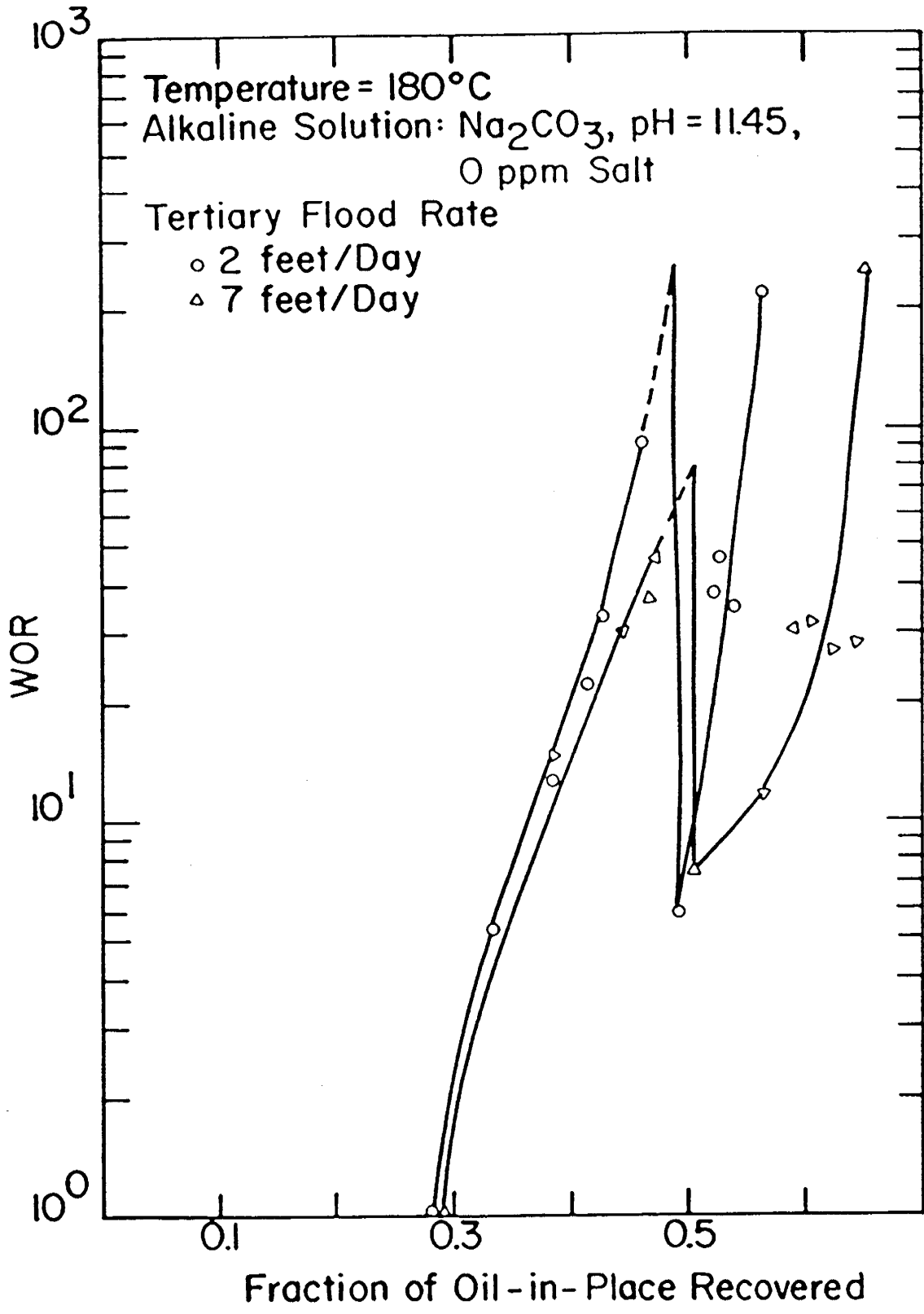


Figure 17 Comparison between WOR curves for sodium carbonate floods at different tertiary flood rates at 180°C

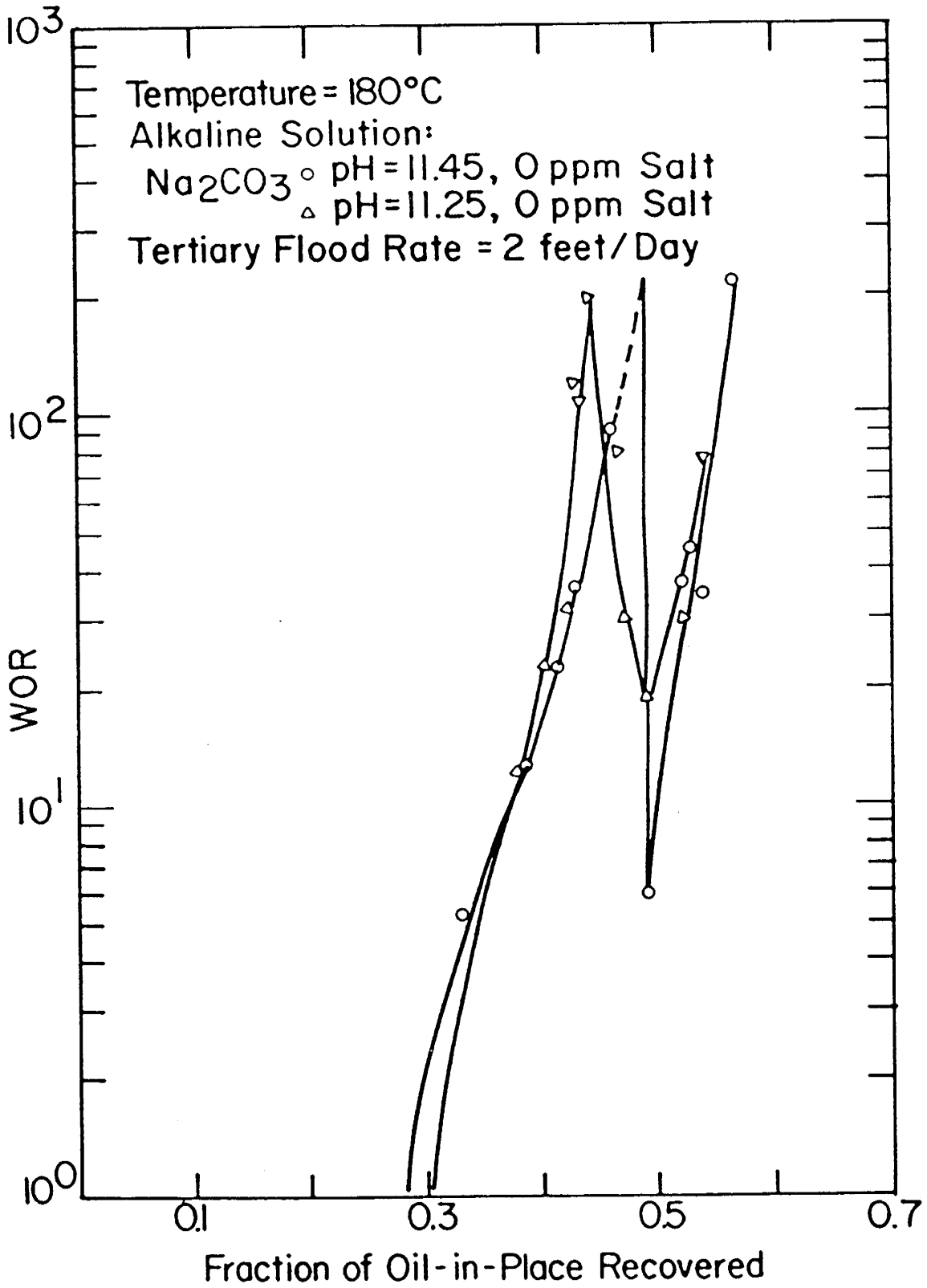


Figure 18 Comparison between WOR curves for sodium carbonate floods at different injection pH's at 180°C

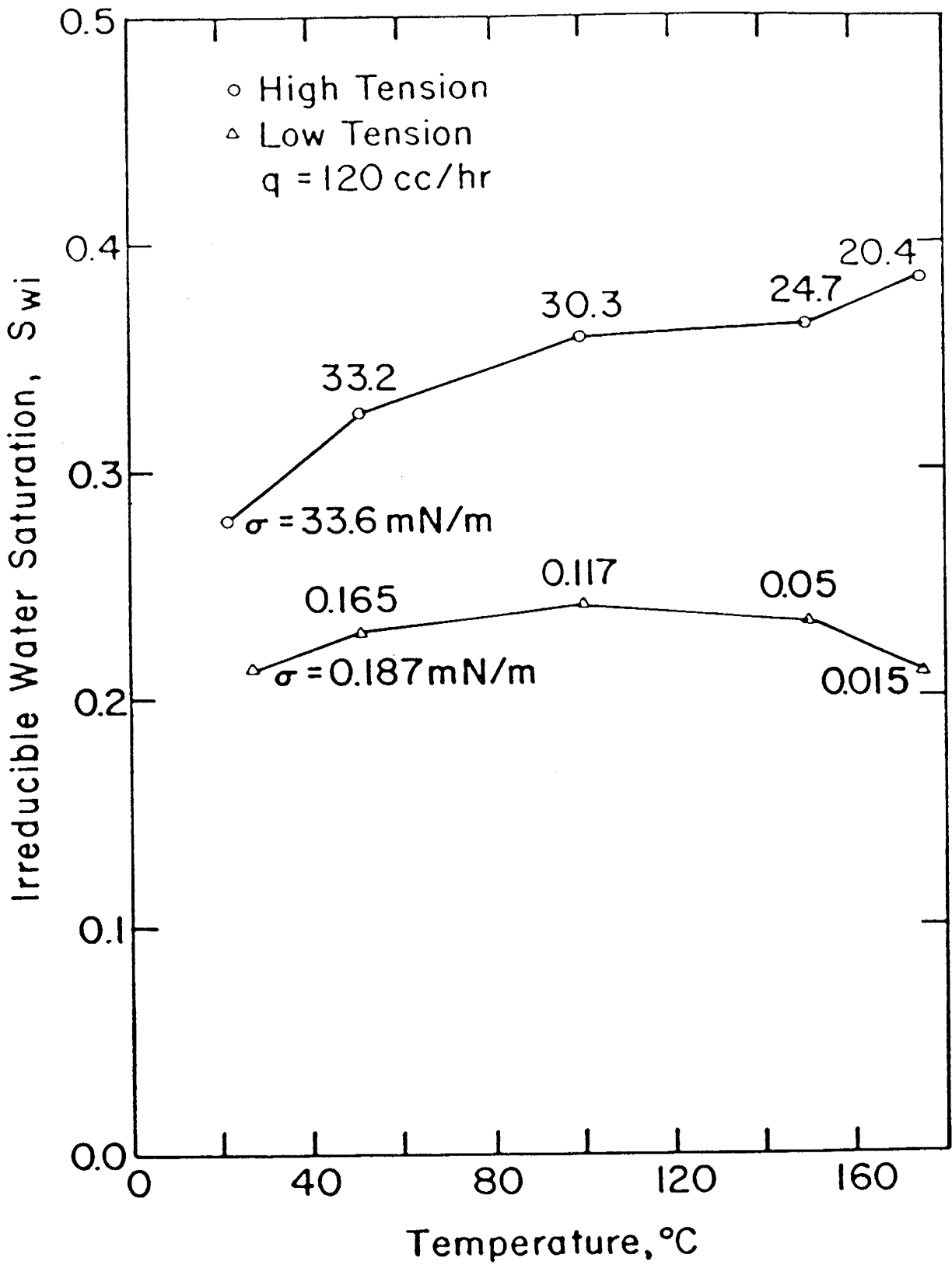


Figure 19 Irreducible water saturation vs. temperature

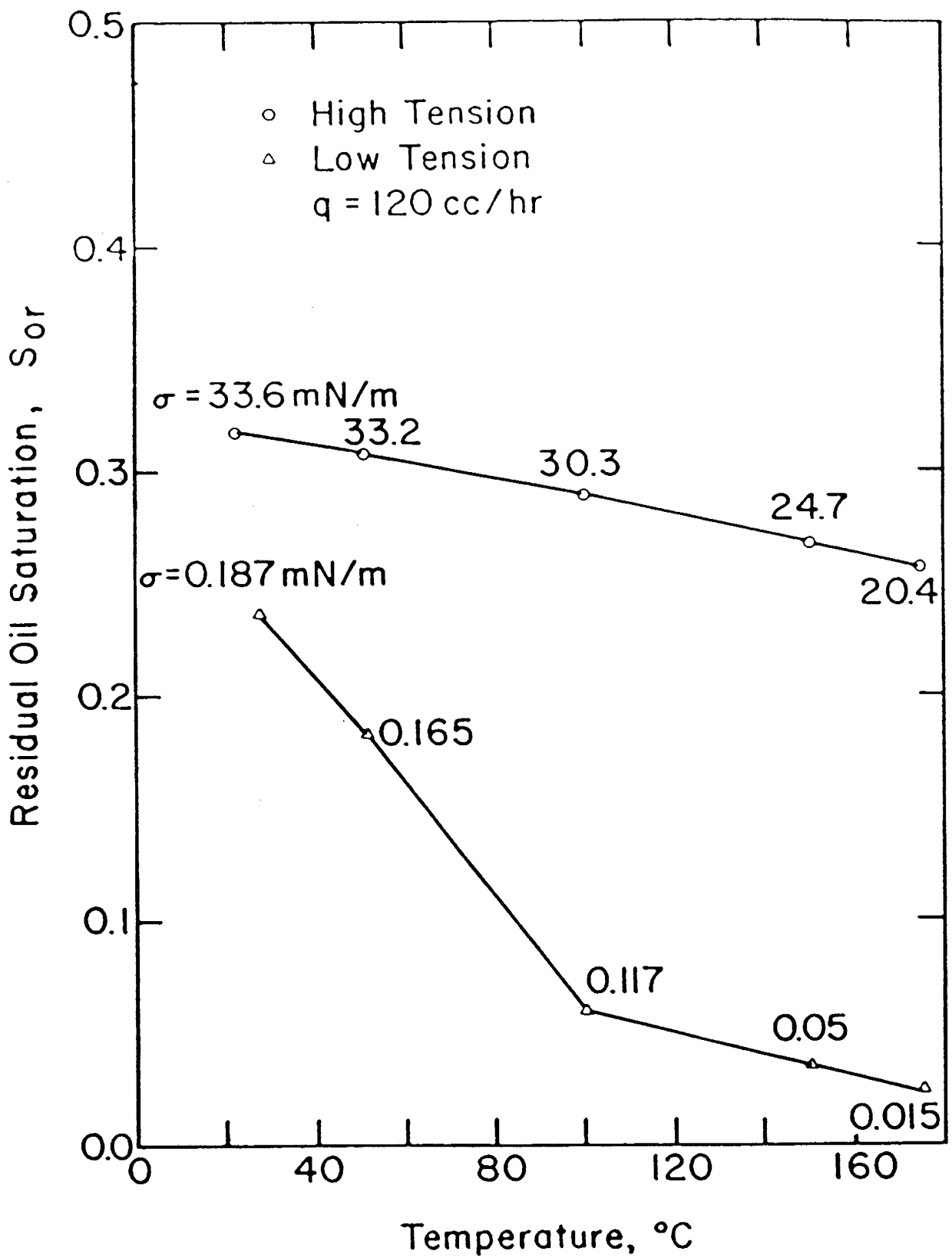


Figure 20 Steady-state residual oil saturation vs. temperature

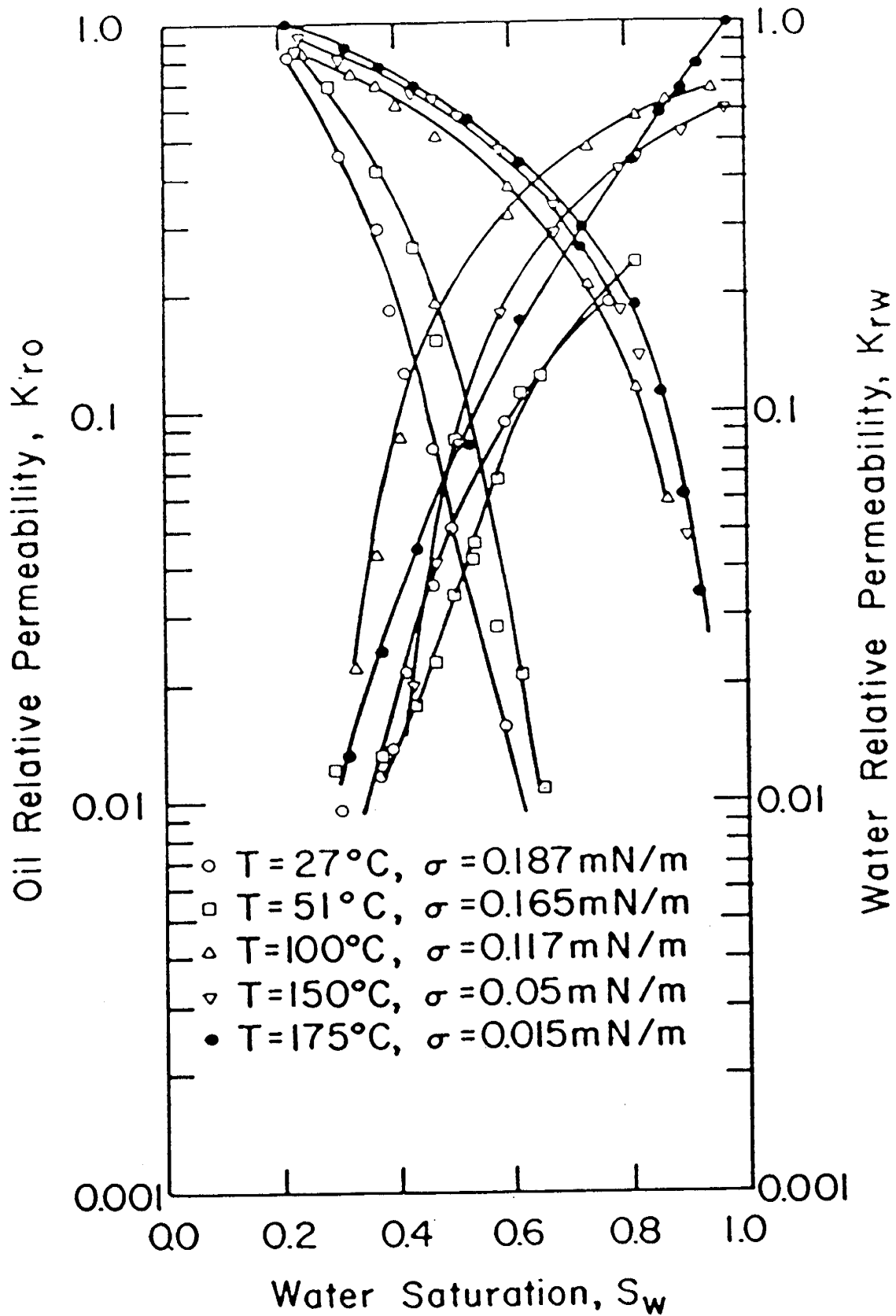


Figure 21 Steady-state imbibition water-oil relative permeability curves at elevated temperatures (low-tension)

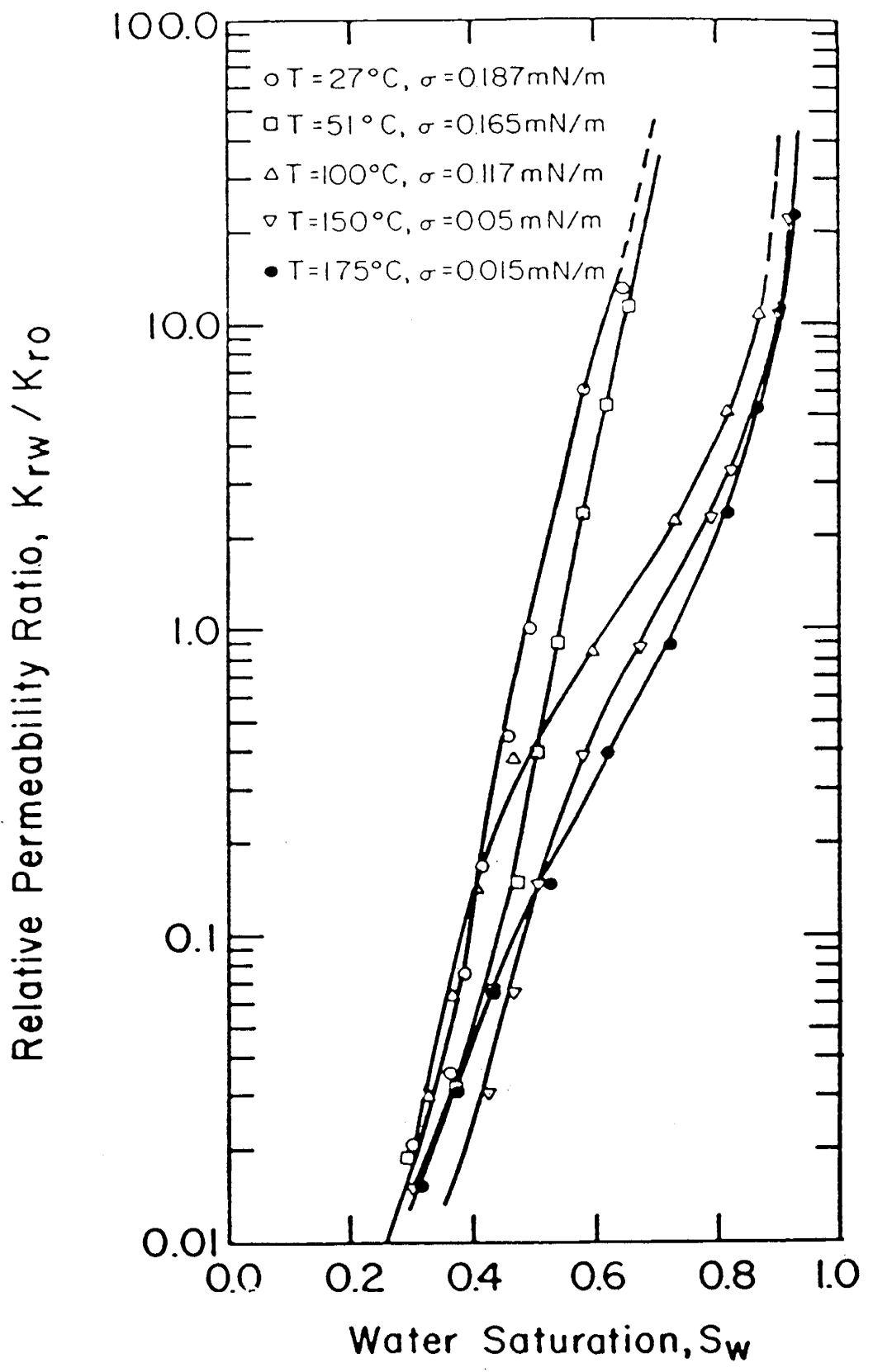


Figure 22 Water/oil relative permeability ratios at elevated temperatures (low-tension)

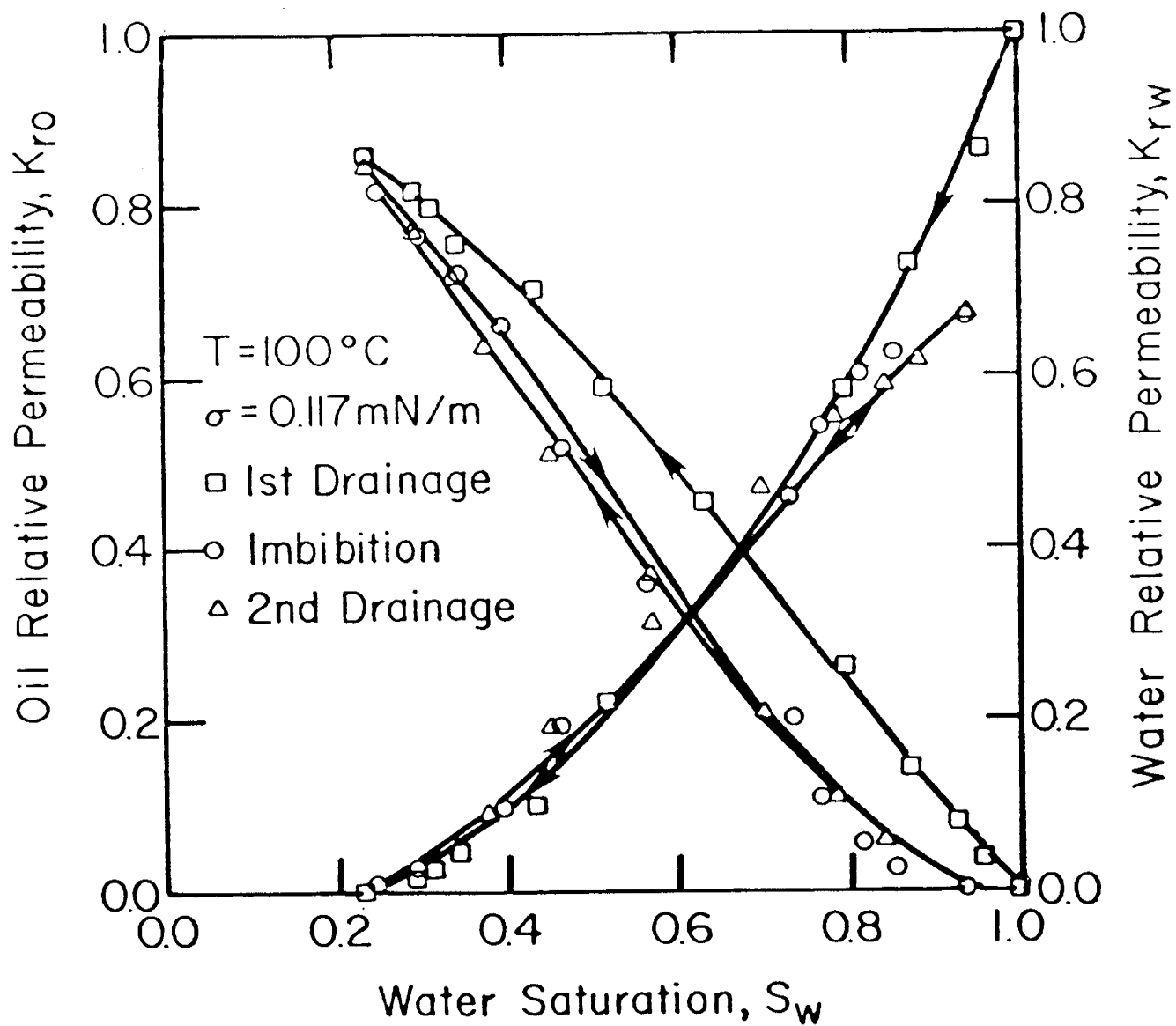


Figure 23 Hysteresis effect on relative permeability curves
 ($T=100^{\circ}\text{C}$, $\sigma=0.117\text{ mN/m}$)

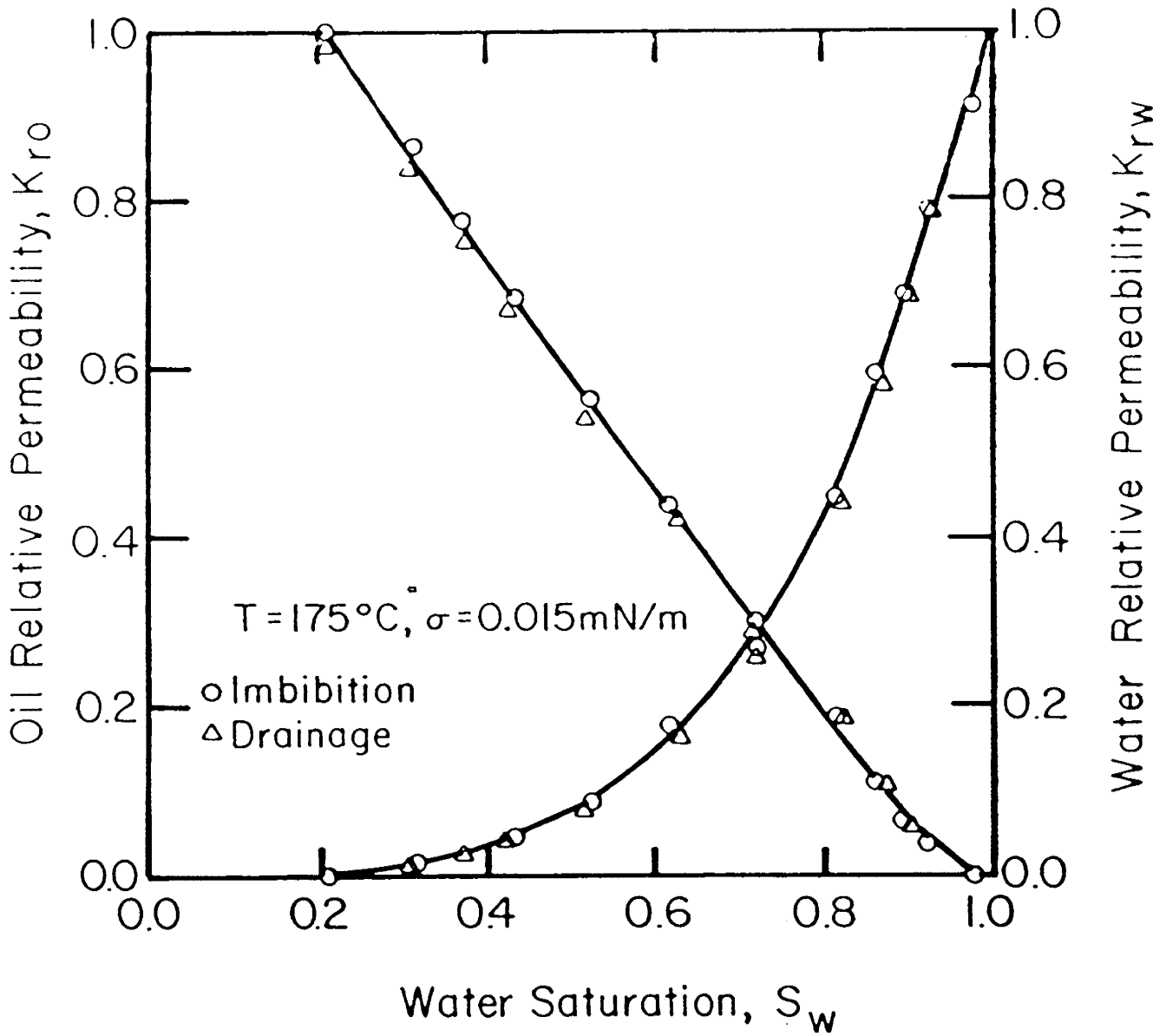


Figure 24 Hysteresis effect on relative permeability curves
($T=175^{\circ}\text{C}, \sigma=0.015 \text{ mN/m}$)

LIST OF PUBLICATIONS

The following thesis was completed under this contract during 1984.

"The Effect of Temperature and Interfacial Tension on Water-Oil Relative Permeabilities of Consolidated Sands"

Torabzadeh, Syed Jalal.

July 11, 1984

Papers Presented or Published

1. Karakas, M., Saneie, S., and Yortsos, Y.C., "Displacement of a Viscous Oil by the Combined Injection of Hot Water and Chemical Additive" SPE 12560 presented at California Regional Meeting April 11-13, 1984.
2. Kumar, S., Torabzadeh, S.J. and Handy, L.L.: "Relative Permeability Functions for High and Low Tension Systems at Elevated Temperatures" SPE 13670 presented at California Regional Meeting in Bakersfield, CA March 27-29, 1985.
3. Mehdizadeh, A. and Handy, L.L.: "Further Investigation of High-Temperature Alkaline Floods" SPE 13072 presented at 59th Annual Technical Conference and Exhibition at Houston, TX Sept. 11-19, 1984.

4. Torabzadeh, S.J. and Handy, L.L.: "The Effect of Temperature and Interfacial Tension on Water-Oil Relative Permeabilities of Consolidated Sands" SPE 12689 presented at SPE/DOE Fourth Symposium on Enhanced Oil Recovery, Tulsa, OK April 15-18, 1984.

